

# FSP1 is a glutathione-independent ferroptosis suppressor

<https://doi.org/10.1038/s41586-019-1707-0>

Received: 25 February 2019

Accepted: 9 October 2019

Published online: 21 October 2019

Sebastian Doll<sup>1,13</sup>, Florencio Porto Freitas<sup>2,13</sup>, Ron Shah<sup>3</sup>, Maceler Aldrovandi<sup>1,4</sup>, Milene Costa da Silva<sup>1</sup>, Irina Ingold<sup>1</sup>, Andrea Goya Grocin<sup>5</sup>, Thamara Nishida Xavier da Silva<sup>2</sup>, Elena Panzilius<sup>6</sup>, Christina H. Scheel<sup>6,7</sup>, André Mourão<sup>8</sup>, Katalin Buday<sup>1</sup>, Mami Sato<sup>1</sup>, Jonas Wanninger<sup>1</sup>, Thibaut Vignane<sup>1</sup>, Vaishnavi Mohana<sup>1</sup>, Markus Rehberg<sup>9</sup>, Andrew Flatley<sup>10</sup>, Aloys Schepers<sup>10</sup>, Andreas Kurz<sup>11</sup>, Daniel White<sup>4</sup>, Markus Sauer<sup>11</sup>, Michael Sattler<sup>8</sup>, Edward William Tate<sup>5</sup>, Werner Schmitz<sup>12</sup>, Almut Schulze<sup>12</sup>, Valerie O'Donnell<sup>4</sup>, Bettina Proneth<sup>1</sup>, Grzegorz M. Popowicz<sup>8</sup>, Derek A. Pratt<sup>3</sup>, José Pedro Friedmann Angeli<sup>2\*</sup> & Marcus Conrad<sup>1\*</sup>

Ferroptosis is an iron-dependent form of necrotic cell death marked by oxidative damage to phospholipids<sup>1,2</sup>. To date, ferroptosis has been thought to be controlled only by the phospholipid hydroperoxide-reducing enzyme glutathione peroxidase 4 (GPX4)<sup>3,4</sup> and radical-trapping antioxidants<sup>5,6</sup>. However, elucidation of the factors that underlie the sensitivity of a given cell type to ferroptosis<sup>7</sup> is crucial to understand the pathophysiological role of ferroptosis and how it may be exploited for the treatment of cancer. Although metabolic constraints<sup>8</sup> and phospholipid composition<sup>9,10</sup> contribute to ferroptosis sensitivity, no cell-autonomous mechanisms have been identified that account for the resistance of cells to ferroptosis. Here we used an expression cloning approach to identify genes in human cancer cells that are able to complement the loss of GPX4. We found that the flavoprotein apoptosis-inducing factor mitochondria-associated 2 (*AIFM2*) is a previously unrecognized anti-ferroptotic gene. *AIFM2*, which we renamed ferroptosis suppressor protein 1 (FSP1) and which was initially described as a pro-apoptotic gene<sup>11</sup>, confers protection against ferroptosis elicited by *GPX4* deletion. We further demonstrate that the suppression of ferroptosis by FSP1 is mediated by ubiquinone (also known as coenzyme Q<sub>10</sub>, CoQ<sub>10</sub>): the reduced form, ubiquinol, traps lipid peroxy radicals that mediate lipid peroxidation, whereas FSP1 catalyses the regeneration of CoQ<sub>10</sub> using NAD(P)H. Pharmacological targeting of FSP1 strongly synergizes with GPX4 inhibitors to trigger ferroptosis in a number of cancer entities. In conclusion, the FSP1–CoQ<sub>10</sub>–NAD(P)H pathway exists as a stand-alone parallel system, which co-operates with GPX4 and glutathione to suppress phospholipid peroxidation and ferroptosis.

Ferroptosis is controlled by the selenoenzyme GPX4<sup>3,4,12</sup>. With the recognition that targeting ferroptosis may help to eradicate therapy-resistant tumours in patients<sup>13–15</sup>, there is mounting interest in understanding the mechanisms that underpin the sensitivity of cells to ferroptosis<sup>16</sup>. Although acyl-CoA synthetase long chain family member 4 (ACSL4) was identified as a pro-ferroptotic gene, the expression of which determines ferroptosis sensitivity<sup>9,10</sup>, inhibition of GPX4 fails to trigger ferroptosis in some cancer cell lines regardless of ACSL4 expression, suggesting that there are alternative resistance mechanisms.

## Genetic suppressor screen uncovers FSP1

To uncover these factors, we generated a cDNA expression library derived from the MCF7 ferroptosis-resistant cell line<sup>9,10</sup> (Extended Data Fig. 1a), and screened for genes complementing loss of *GPX4* (Fig. 1a). Sequencing of 14 single-cell clones identified 7 clones that express either *GPX4* or *AIFM2* (Extended Data Fig. 1b). *AIFM2* is a flavoprotein that has originally been described as a p53-responsive gene<sup>17</sup> and claimed to induce apoptosis based on sequence similarity to another initially postulated pro-apoptotic gene,

<sup>1</sup>Institute of Developmental Genetics, Helmholtz Zentrum München, Neuherberg, Germany. <sup>2</sup>Rudolf Virchow Center for Experimental Biomedicine, University of Würzburg, Würzburg, Germany. <sup>3</sup>Department of Chemistry & Biomolecular Sciences, University of Ottawa, Ottawa, ON, Canada. <sup>4</sup>Systems Immunity Research Institute, School of Medicine, Cardiff University, Cardiff, UK.

<sup>5</sup>Molecular Sciences Research Hub, Department of Chemistry, Imperial College London, London, UK. <sup>6</sup>Institute of Stem Cell Biology, Helmholtz Zentrum München, Neuherberg, Germany.

<sup>7</sup>Clinic for Dermatology, St Josef Hospital Bochum, University of Bochum, Bochum, Germany. <sup>8</sup>Institute of Structural Biology, Helmholtz Zentrum München, Neuherberg, Germany. <sup>9</sup>Institute of Lung Biology and Disease, Helmholtz Zentrum München, Neuherberg, Germany. <sup>10</sup>Monoclonal Antibody Core Facility, Helmholtz Zentrum München, Neuherberg, Germany. <sup>11</sup>Department of Biotechnology & Biophysics, Biocenter, University of Würzburg, Würzburg, Germany. <sup>12</sup>Department of Biochemistry and Molecular Biology, Theodor Boveri Institute, Biocenter, University of Würzburg, Würzburg, Germany. <sup>13</sup>These authors contributed equally: Sebastian Doll, Florencio Porto Freitas. \*e-mail: pedro.angeli@virchow.uni-wuerzburg.de; marcus.conrad@helmholtz-muenchen.de

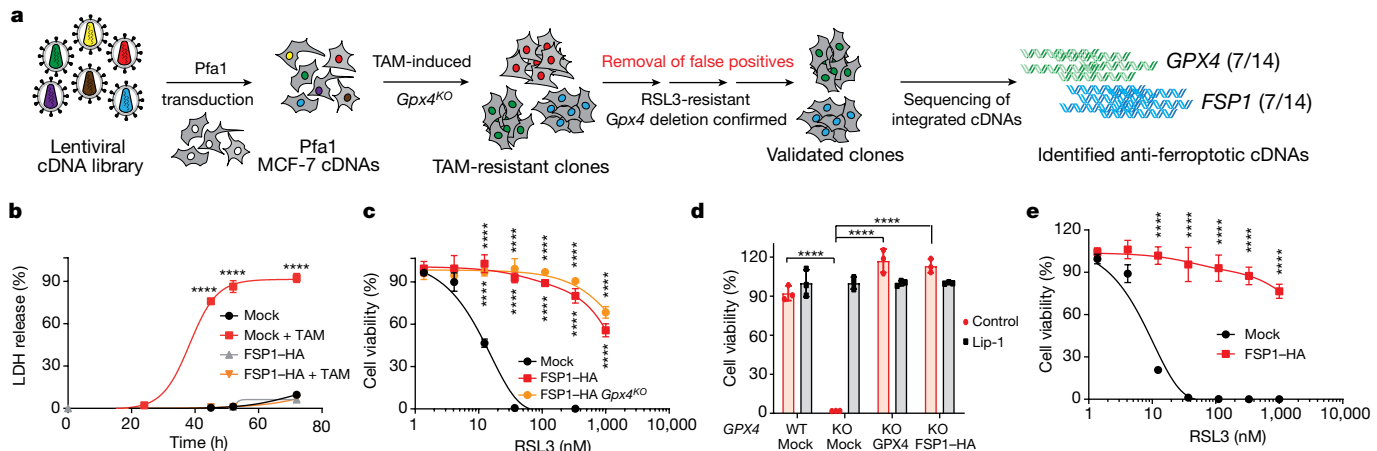


**Fig. 1 | Identification and validation of FSP1 as a ferroptosis suppressor.**

**a**, Schematic of the identification of FSP1 as a ferroptosis suppressor, using double selection with 4-hydroxytamoxifen (TAM)-induced *Gpx4*-knockout (KO) followed by RSL3-mediated elimination of false-positive cell clones. Surviving single-cell clones were analysed by Sanger sequencing. **b**, Cell death induced by TAM was measured by lactate dehydrogenase (LDH) release of Pfa1 cells stably expressing an empty vector (mock) and FSP1 tagged with haemagglutinin (FSP1-HA) using supernatants collected at the indicated time points in a 96-well plate. **c–e**, Dose-dependent toxicity of RSL3-induced cell

death of Pfa1 *Gpx4* wild-type (WT) or *Gpx4*-knockout for cells expressing mock or FSP1-HA (**c**), *GPX4* wild-type and *GPX4*-knockout HT1080 cells overexpressing mock, human GPX4-FSH (Flag-Strep-His-tag) or FSP1-HA treated with or without 200 nM liproxstatin-1 (Lip-1; **d**) and HT1080 cells expressing mock or FSP1-HA (**e**). Cell viability was assessed 24 h (**c**, **e**) or 72 h (**d**) thereafter using Aquabluer. Data are the mean  $\pm$  s.d. of  $n = 3$  wells of a 96-well plate from one representative of two (**b**) or three (**c–e**) independent experiments; \*\*\* $P < 0.0001$ ; two-way analysis of variance (ANOVA).

apoptosis-inducing factor mitochondria-associated 1 (AIFM1)<sup>11</sup>. To avoid further confusion, we therefore recommend that in the future AIFM2 is referred to as ferroptosis suppressor protein 1 (FSP1)<sup>18</sup>. For validation, we stably expressed FSP1 in mouse Pfa1<sup>19</sup> and in human fibrosarcoma HT1080 cells (Extended Data Fig. 1c, d). FSP1-overexpressing cells were robustly protected against pharmacological and genetic inducers of ferroptosis<sup>1</sup> and proliferated indefinitely (Fig. 1b–e, Extended Data Fig. 1e–i and Supplementary Video 1). To our knowledge, this is the first enzymatic system that complements loss of *GPX4*<sup>19</sup>.

The anti-ferroptotic function of FSP1 was found to be independent of cellular glutathione levels, GPX4 activity, ACSL4 expression and oxidizable fatty acid content (Extended Data Figs. 1c, d, j, k, 2), showing that FSP1 does not interfere with canonical ferroptosis mechanisms. Moreover, the protection against cell death conferred by FSP1 was specific to ferroptosis-inducing agents; FSP1 did not protect against cell death caused by cytotoxic compounds and/or pro-apoptotic conditions. Moreover, p53 status did not affect FSP1 expression (Extended Data Fig. 3a–e). In contrast to FSP1, overexpression of AIFM1 failed to suppress ferroptosis (Extended Data Fig. 3f, g).

## N-myristoylation enables ferroptosis resistance

Our early efforts revealed that N-terminal tagging of FSP1 abolished its anti-ferroptotic activity. Indeed, the N terminus of FSP1 contains a canonical myristoylation motif<sup>20</sup>, which presumably facilitates its association with lipid bilayers<sup>21</sup>. Expression of wild-type FSP1 and a mutant form of FSP1 that lacks the predicted myristoylation site (G2A) in Pfa1 and HT1080 cells (Fig. 2a), as well as FSP1 tagging with an alkyne-functionalized myristic acid mimetic (YnMyr) enabled the specific enrichment of only wild-type FSP1. This enrichment was abolished either in FSP1(G2A) mutants or after treatment with the pan-N-myristoyl transferase inhibitor IMP-1088<sup>22</sup> (Fig. 2b). Myristoylation of FSP1 appears to be essential for its anti-ferroptotic activity as FSP1(G2A)- and wild-type FSP1-expressing cells treated with IMP-1088 showed abrogated ferroptosis resistance (Fig. 2c, d and Extended Data Fig. 3h, i). We therefore assessed the subcellular

distribution of both wild-type FSP1 and FSP1(G2A) using C-terminally tagged fusion proteins. Although FSP1-GFP localized to an unspecified perinuclear membrane compartment, it also partially overlapped with endoplasmic reticulum and Golgi markers (Fig. 2e and Extended Data Fig. 4a). By contrast, FSP1(G2A)-GFP was distributed throughout the cell, suggesting that ferroptosis is perhaps driven in a specific subcellular region. A more in-depth investigation of the subcellular localization of FSP1 is provided in a companion study<sup>18</sup> that reveals a notable role of plasma membrane-targeted FSP1 in the suppression of ferroptosis.

## FSP1 prevents lipid peroxidation

As ferroptosis is driven by phospholipid peroxidation (pLPO), we stained Pfa1 cells with BODIPY 581/591 C11 and found that FSP1 overexpression blunted lipid peroxidation induced by (1S, 3R)-RSL3 (RSL3; Fig. 3a). Moreover, specific pLPO products were markedly lower in *Gpx4*-knockout FSP1-overexpressing cells (Fig. 3b and Extended Data Fig. 4b). As members of the AIF family have been shown to possess NADH:ubiquinone oxidoreductase activity<sup>23</sup>, we hypothesized that FSP1 suppresses pLPO by regenerating lipophilic radical-trapping antioxidants using NAD(P)H. The reduced form of coenzyme Q<sub>10</sub> (CoQ<sub>10</sub>-H<sub>2</sub>) has been reported to be a good radical-trapping antioxidant in phospholipids and lipoproteins<sup>24</sup>, yet is considered to be of limited importance outside mitochondria, as an efficient recycling mechanism has not been described. To investigate a possible link between FSP1 and CoQ<sub>10</sub>-H<sub>2</sub>, we generated CoQ<sub>10</sub>-deficient HT1080 cells by deleting 4-hydroxybenzoate polyprenyltransferase (COQ2), the enzyme that catalyses the first step in CoQ<sub>10</sub> biosynthesis (Fig. 3c). CoQ<sub>10</sub>-deprived cells proliferated normally when supplemented with uridine, CoQ<sub>10</sub> or decyl-ubiquinone (Extended Data Fig. 4c). Notably, whereas FSP1-GFP overexpression in parental HT1080 cells suppressed ferroptosis, it failed to do so in *Coq2*-knockout cells (Fig. 3d and Extended Data Fig. 4d). Consistent with previous data that have shown that purified FSP1 reduces ubiquinone analogues of variable chain lengths<sup>23</sup>, heterologously expressed FSP1 (Extended Data Fig. 4e) catalysed the reduction of an ubiquinone analogue with an appended coumarin fluorophore. This enabled

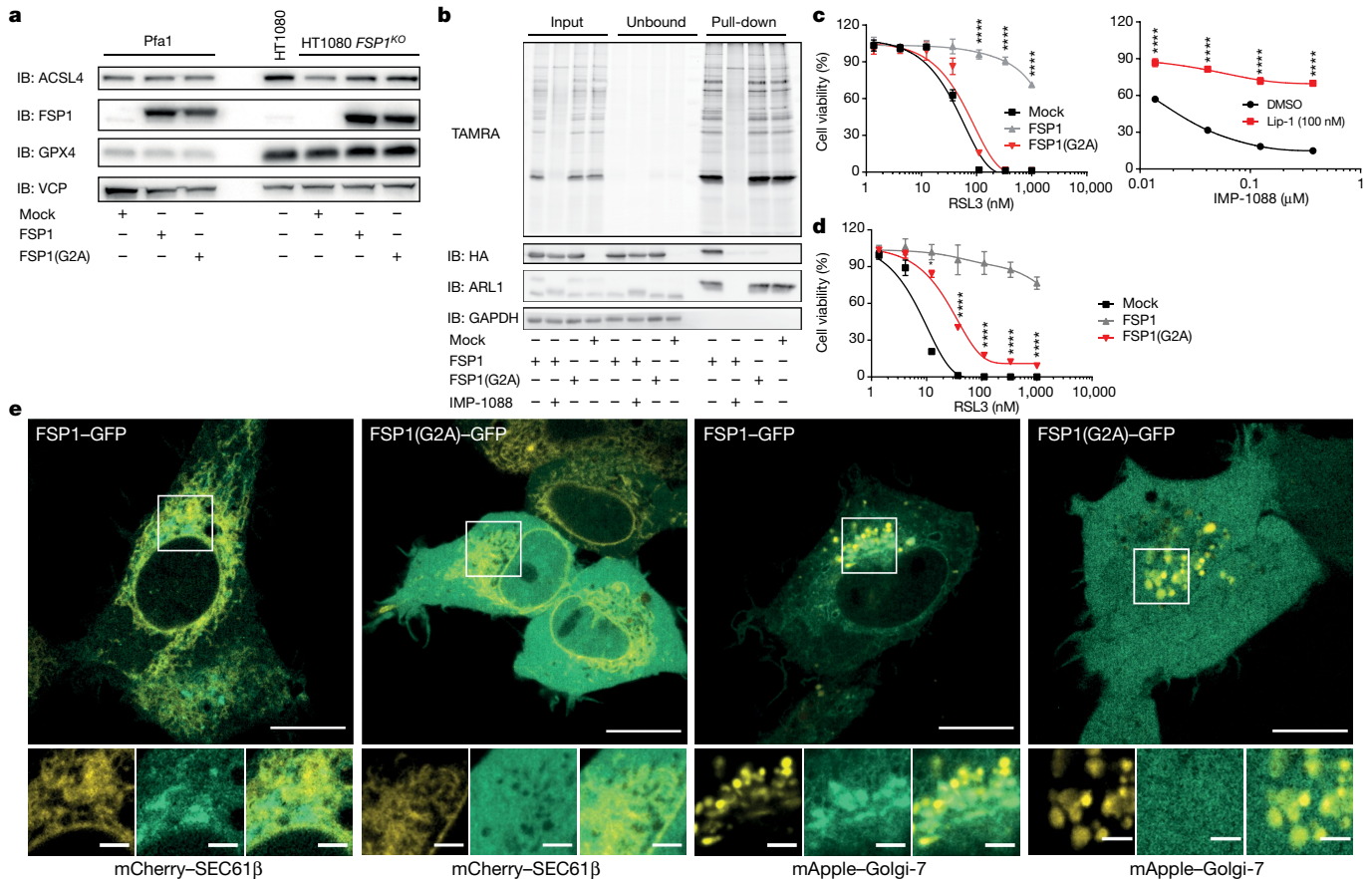


**Fig. 2 | N-Myristylation of FSP1 is important for its anti-ferroptotic function.** **a**, Immunoblotting (IB) analysis of ACSL4, FSP1, GPX4 and valosin-containing protein (VCP) expression of Pfa1 cells stably expressing mock, FSP1-HA or FSP1(G2A)-HA (left), parental HT1080 cells and FSP1-knockout HT1080 cells stably expressing mock, FSP1-HA or FSP1(G2A)-HA (right). Immunoblot images are cropped from the chemiluminescence signal files. For gel source data showing the overlap of colorimetric and chemiluminescence signals, see Supplementary Fig. 1. **b**, Specific enrichment of myristoylated proteins using metabolic labelling with the YnMyr myristate analogue followed by click chemistry to AzTB (Pfa1 FSP1-HA, Pfa1 FSP1-HA and IMP-1088, Pfa1 FSP1(G2A)-HA, Pfa1 mock). TAMRA in-gel fluorescence showing labelling of myristoylated proteins. FSP1 was specifically enriched with YnMyr and the enrichment was prevented by the pan-myristylation inhibitor IMP-1088 as well as by the FSP1(G2A) mutant, demonstrated by immunoblot analysis (HA antibody). Endogenously expressed ADP ribosylation factor-like GTPase 1 (ARL1), served as positive control and glyceraldehyde-3-phosphate dehydrogenase (GAPDH) as loading control. Immunoblot images are cropped from the chemiluminescence signal files.

For gel source data showing the Cy5 ladder and chemiluminescence signals separately, see Supplementary Fig. 1. **c**, Left, dose-dependent toxicity of RSL3 in Pfa1 cells stably expressing mock, FSP1-HA or FSP1(G2A)-HA. The FSP1(G2A) mutant failed to prevent RSL3-induced ferroptosis. Right, inhibition of myristylation (IMP-1088) in FSP1-overexpressing *Gpx4*-knockout Pfa1 cells induced cell death in a dose-dependent manner, which was prevented by the ferroptosis inhibitor Lip-1. **d**, RSL3-induced cell death of FSP1-knockout HT1080 cells stably expressing mock, FSP1 or FSP1(G2A). Cell viability was assessed after 24 h using Aquabluer (**c**, **d**). Data are the mean  $\pm$  s.d. of  $n = 4$  (**c**, left) or  $n = 3$  (**c**, right; **d**) wells of a 96-well plate from one representative of three (**c**, **d**) independent experiments. \*\*\*\* $P < 0.0001$ ; two-way ANOVA. **e**, Enhanced resolution confocal microscopy of HT1080 cells (FSP1-GFP or FSP1(G2A)-GFP) overexpressing mCherry-Sec61 $\beta$  (endoplasmic reticulum localization) or mApple-Golgi-7 (Golgi localization). GFP is displayed in green; mCherry and mApple fluorescence are pseudo-coloured in yellow. Scale bars, 10  $\mu$ m (top) and 2  $\mu$ m (bottom, magnified images).

the determination of kinetic parameters for FSP1, which revealed a relatively low Michaelis constant ( $K_m = 1.2 \times 10^{-5}$  M) and much higher maximum rate of the reaction ( $V_{max} = 4.1 \times 10^{-7}$  M s $^{-1}$ ) compared to related oxidoreductases (for example, NQO1 ( $K_m = 7.9 \times 10^{-7}$  M and  $V_{max} = 6.1 \times 10^{-9}$  M s $^{-1}$ )), as well as the expected inhibition of the substrate (Fig. 3e). Notably, we found that dehydroascorbate, oxidized glutathione and tert-butyl hydroperoxide did not act as substrates of FSP1 (Fig. 3f).

To further investigate our hypothesis that FSP1 suppresses pLPO by reducing CoQ<sub>10</sub>, we carried out co-autoxidation experiments with egg phosphatidylcholine and STY-BODIPY<sup>25</sup> using a lipophilic alkoxyl radical generator (Extended Data Fig. 5a, b). We found that neither FSP1 alone or in combination with its reducing co-substrate, NAD(P)H, was able to suppress pLPO effectively (Extended Data Fig. 5c), whereas

addition of CoQ<sub>10</sub> substantially delayed the autoxidation of egg phosphatidylcholine in a dose-dependent manner (Extended Data Fig. 5d, e). These results suggest that, through FSP1, CoQ<sub>10</sub> helps to shuttle reducing equivalents from NAD(P)H into the lipid bilayer to inhibit propagation of lipid peroxidation. NQO1 was unable to serve in the same capacity as FSP1 in these assays (Extended Data Fig. 5f, g). As CoQ<sub>10</sub> is readily autoxidized and has poor dynamics within the lipid bilayer<sup>26</sup>, we wondered whether  $\alpha$ -tocopherol may also contribute to the protection against ferroptosis observed by FSP1-CoQ<sub>10</sub>. Therefore, after its reaction with a lipid-derived peroxy radical,  $\alpha$ -tocopherol could either be regenerated by reduced CoQ<sub>10</sub> or directly *in vitro* by FSP1 without the need for CoQ<sub>10</sub> (Extended Data Fig. 5h–j). Direct monitoring of phospholipid hydroperoxide formation in linoleate-rich liposomes corroborated the results of the co-autoxidation experiments, showing

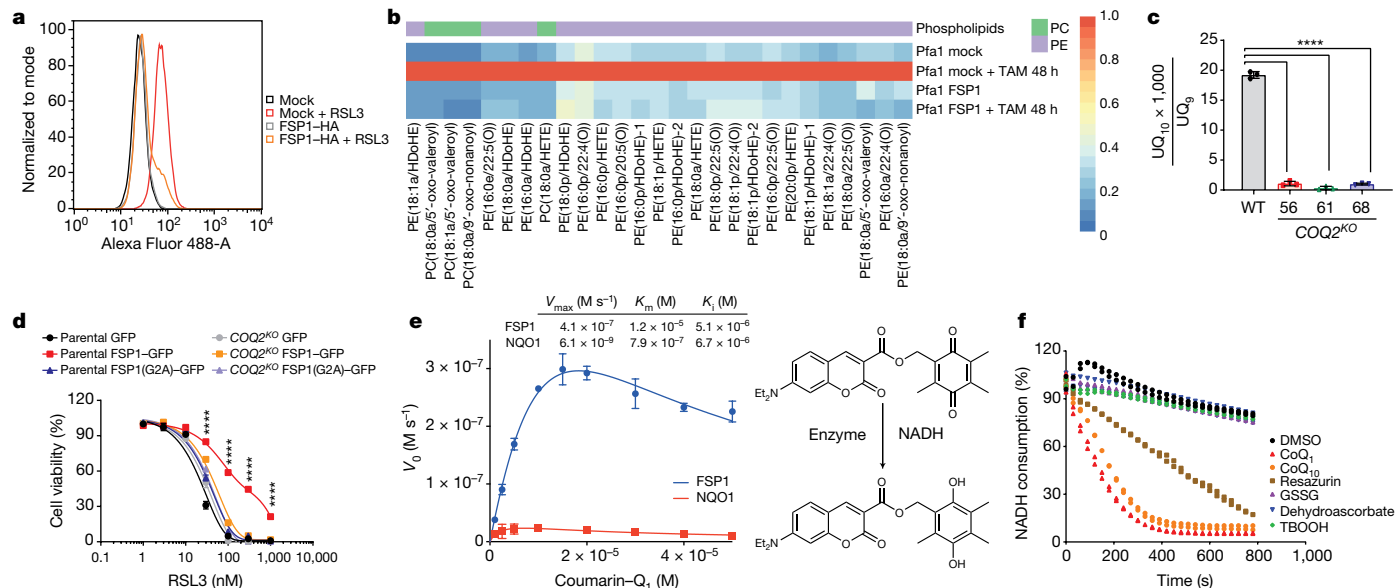


**Fig. 3 | FSP1 protects cells against unrestrained lipid peroxidation.** **a**, Flow cytometry analysis of RSL3-induced (300 nM for 3 h) BODIPY 581/591 C11 oxidation in Pfa1 cells overexpressing mock or FSP1-HA. Data show one representative of two independently performed experiments. **b**, Heat map showing the representation of mono-oxidized phospholipid species (PE, phosphatidylethanolamines; PC, phosphatidylcholine) in mock and FSP1-HA-expressing Pfa1 cells treated with or without 4-hydroxytamoxifen (TAM) for 48 h. For the heat map, samples ( $n = 6$ ) were averaged and normalized to cell number ( $1 \times 10^6$  cells). Each lipid species was normalized to the maximum detected level. The experiment was performed independently twice. **a**, acyl; **e**, plasmanyl; p, plasmenyl/plasmalogen. **c**, Relative quantification of ubiquinone  $CoQ_{10}$  ( $[M + NH_4]^+$   $m/z = 880.7177$ , retention time = 22.8 min) in parental HT1080 and  $COQ2$ -knockout HT1080 clones using liquid chromatography–mass spectrometry. Ubiquinone 9 ( $[M + NH_4]^+$   $m/z = 812.6551$ , retention time = 12.3 min) was used as internal standard. **d**, Dose-dependent toxicity of RSL3 in parental and  $COQ2$ -knockout HT1080

cells overexpressing FSP1-GFP, FSP1(G2A)-GFP or GFP. Cell viability was assessed after 24 h using Aquabluer. **e**, Kinetic parameters for the reduction of coumarin-quinone ( $Q_1$ ) conjugate by FSP1 (50 nM, blue) and NQO1 (50 nM, red) in Tris-buffered saline (10 mM, pH 7.4) in the presence of NADH (200  $\mu$ M) at 37 °C. Initial rates were determined from the fluorescence of the product hydroquinone (excitation, 415 nm; emission, 470 nm). The data are fitted to a standard substrate inhibition model and are mean  $\pm$  s.d. **f**, NADH consumption assay (340 nm) in TBS buffer using recombinant purified human FSP1 in combination with different electron acceptor molecules (ubiquinone-1 ( $CoQ_1$ ), ubiquinone-10 ( $CoQ_{10}$ ), resazurin, oxidized glutathione (GSSG), dehydroascorbate and tert-butyl hydroperoxide (TBOOH)). Data represent  $n = 2$  technical replicates of one out of three independent experiments (**f**). Data are mean  $\pm$  s.d. of  $n = 4$  (**d**) or  $n = 3 (**c**, **e**) wells of a 96-well plate from one representative of three (**e**) or one (**c**, **d**) independent experiments, *** $P < 0.0001$ ; one-way ANOVA (**c**) and two-way ANOVA (**d**).$

substantial FSP1-catalysed suppression of pLPO that was further enhanced in the presence of both  $CoQ_{10}$  and  $\alpha$ -tocopherol (Extended Data Fig. 5k).

### Loss of FSP1 sensitizes to ferroptosis

On the basis of the strong protective effect provided by FSP1 and the possibility to maintain cells in the absence of GPX4, we imagined that a counter-screen of FSP1-overexpressing cells in a GPX4 knockout or wild-type background could be useful for the discovery of FSP1 inhibitors. We screened approximately 10,000 drug-like compounds<sup>4</sup>, which led to the identification of iFSP1 as a potent FSP1 inhibitor (Fig. 4a). iFSP1 selectively induced ferroptosis in GPX4-knockout Pfa1 and HT1080 cells that overexpressed FSP1 (Extended Data Fig. 6a, b). Preliminary structure–activity relationship studies have yet to identify compounds with substantial improvement over iFSP1 (Extended Data Fig. 6c).

To determine whether FSP1 could serve as a ferroptosis suppressor in cancer, we generated a monoclonal antibody against human FSP1 (Extended Data Fig. 6d), and explored its expression along with the main ferroptosis players in a panel of human cancer cell lines of different origins (Extended Data Fig. 7). Indeed, FSP1 was expressed in most tumour cell lines, and iFSP1 treatment robustly sensitized these cells to RSL3-induced ferroptosis (Extended Data Fig. 8). We then generated FSP1-knockout and FSP1-overexpressing cells from a selection of these cell lines (Fig. 4b, c and Extended Data Fig. 7) and compared the effects of pharmacological inhibition (iFSP1) and FSP1

knockout on the sensitization of cells to ferroptosis. As expected, genetic deletion of *FSP1* was more efficient than small-molecule inhibition, whereas iFSP1 treatment in the *FSP1*-knockout background had no additive effect to RSL3-induced ferroptosis (Extended Data Fig. 6e, f). Notably, a few cells that were sensitive to RSL3 could not be resensitized by iFSP1 when FSP1 was overexpressed. This may be due to drug metabolism and excretion, and these effects should be investigated further (Extended Data Fig. 6f). Detailed experiments demonstrated that *FSP1* knockout in MDA-MB-436 cells lowered their resistance to RSL3-induced ferroptosis, whereas mouse FSP1 re-expression restored the resistance of cells to ferroptosis (Fig. 4d, e). Analysis of the cancer dependency map (DepMap; <https://depmap.org/portal/>) revealed that lower expression of FSP1 correlates with an increased GPX4 dependency in a panel of 559 cancer cell lines (Extended Data Fig. 9a). Additionally, FSP1 expression directly correlated with resistance to ferroptosis inducers RSL3, ML162 and ML210 in a panel of 860 cancer cell lines (<https://portals.broadinstitute.org/ctrp>) (Extended Data Fig. 9b). No synergistic cell death was detected with cisplatin or other known cytotoxic compounds (Extended Data Fig. 9c, d), suggesting that FSP1 inhibition selectively sensitizes cells to ferroptosis inducers. This finding is particularly important as therapy-resistant tumours only respond to complete elimination of GPX4 activity; minute amounts are sufficient to sustain cell viability<sup>27</sup>. Moreover, pharmacological targeting of GPX4 may only achieve partial anti-tumour effects. In fact, in mice bearing human xenografts, a companion study<sup>18</sup> demonstrates that the growth of H460 tumours can only be reduced by concomitant deletion

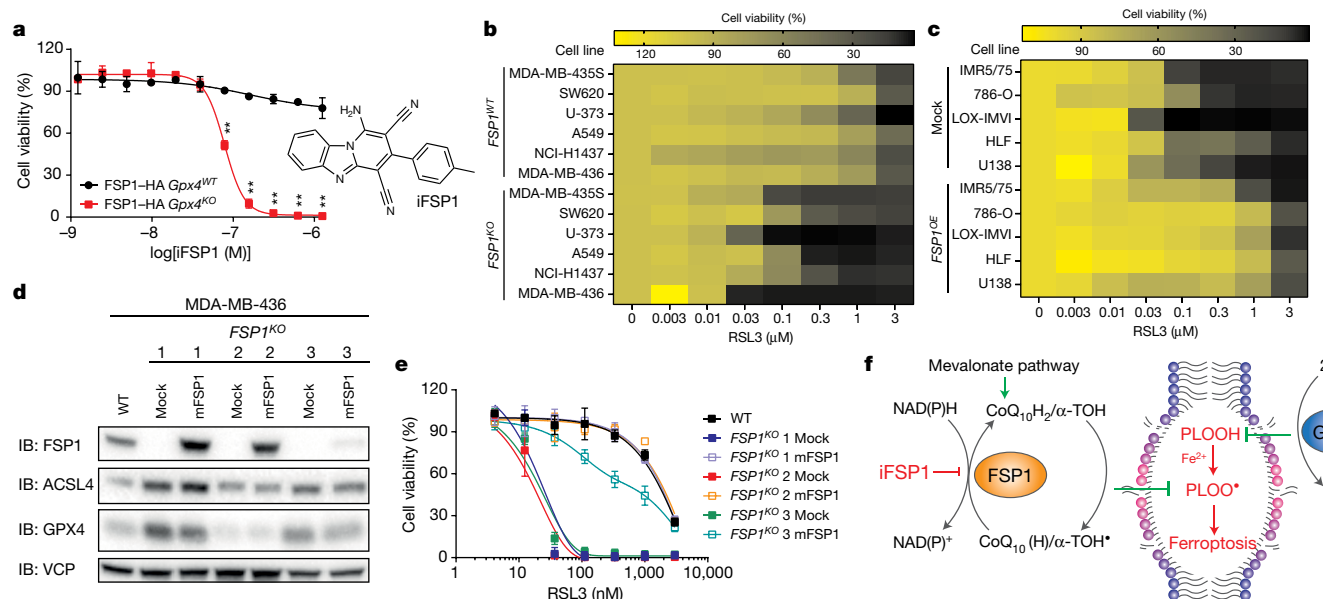


**Fig. 4 | FSP1 inhibition sensitizes tumour cells to ferroptosis.** **a**, Chemical structure of iFSP1. Dose-dependent toxicity of iFSP1 in wild-type and *Gpx4*-knockout Pfal cells overexpressing FSP1-HA. **b, c**, Heat maps depicting the dose-dependent toxicity of RSL3 in a panel of genetically engineered human cancer cell lines (*FSP1* knockout (**b**); *FSP1* overexpression (OE) (**c**); for detailed cell viability assays including iFSP1 and liproxstatin-1 treatments, see Extended Data Fig. 6e, f). **d**, Immunoblot analysis of FSP1, ACSL4, GPX4 and VCP expression in parental MDA-MB-436 cells and three independent *FSP1*-knockout clones (KO 1–3) overexpressing mock or mouse FSP1 (mFSP1). Immunoblot images are cropped from the chemiluminescence signal files. For

gel source data showing the overlap of colorimetric and chemiluminescence signals, see Supplementary Fig. 1. **e**, Dose-dependent toxicity of RSL3 of the cell lines depicted in **d**. Expression of FSP1 restored resistance to RSL3-induced ferroptosis in all three clones. **f**, Graphical abstract depicting the anti-ferroptotic function of FSP1 as a glutathione-independent suppressor of phospholipid peroxidation by inhibition of lipid radical-mediated autoxidation, initiated by peroxy radicals (PLOO<sup>•</sup>), of lipid bilayers. Data are mean  $\pm$  s.d. of  $n = 3$  wells of a 96-well plate from one representative of one (**a**) or two (**b, c, e**) independent experiments; \*\* $P < 0.01$ ; two-way ANOVA.

of *GPX4* and *FSP1*, whereas *GPX4* single-knockout tumours grow normally.

Our data establish that the NADH-FSP1-CoQ<sub>10</sub> pathway is a potent suppressor of pLPO and ferroptosis (Fig. 4f). As such, phospholipid redox homeostasis can be disassociated from the glutathione–GPX4 axis, and can be further exploited pharmacologically to efficiently sensitize cancer cells to ferroptosis inducers. Our discovery explains why NAD(P)H<sup>28</sup> and defects in the mevalonate pathway through loss of ubiquinone<sup>13,29</sup> converge on FSP1 and thereby predict sensitivity to ferroptosis. Furthermore, our data provide a compelling case for the long-debated antioxidant role<sup>30,31</sup> of extra-mitochondrial CoQ<sub>10</sub> and suggest that its beneficial effects should be investigated further alongside FSP1.

## Online content

Any methods, additional references, Nature Research reporting summaries, source data, extended data, supplementary information, acknowledgements, peer review information; details of author contributions and competing interests; and statements of data and code availability are available at <https://doi.org/10.1038/s41586-019-1707-0>.

- Dixon, S. J. et al. Ferroptosis: an iron-dependent form of nonapoptotic cell death. *Cell* **149**, 1060–1072 (2012).
- Conrad, M., Angeli, J. P., Vandenebeele, P. & Stockwell, B. R. Regulated necrosis: disease relevance and therapeutic opportunities. *Nat. Rev. Drug Discov.* **15**, 348–366 (2016).
- Yang, W. S. et al. Regulation of ferroptotic cancer cell death by GPX4. *Cell* **156**, 317–331 (2014).
- Friedmann Angeli, J. P. et al. Inactivation of the ferroptosis regulator Gpx4 triggers acute renal failure in mice. *Nat. Cell Biol.* **16**, 1180–1191 (2014).
- Zilka, O. et al. On the mechanism of cytoprotection by ferrostatin-1 and liproxstatin-1 and the role of lipid peroxidation in ferroptotic cell death. *ACS Cent. Sci.* **3**, 232–243 (2017).
- Shah, R., Shchepinov, M. S. & Pratt, D. A. Resolving the role of lipoxygenases in the initiation and execution of ferroptosis. *ACS Cent. Sci.* **4**, 387–396 (2018).
- Stockwell, B. R. et al. Ferroptosis: a regulated cell death nexus linking metabolism, redox biology, and disease. *Cell* **171**, 273–285 (2017).
- Tarangelo, A. et al. p53 suppresses metabolic stress-induced ferroptosis in cancer cells. *Cell Rep.* **22**, 569–575 (2018).
- Kagan, V. E. et al. Oxidized arachidonic and adrenic PEs navigate cells to ferroptosis. *Nat. Chem. Biol.* **13**, 81–90 (2017).
- Doll, S. et al. ACSL4 dictates ferroptosis sensitivity by shaping cellular lipid composition. *Nat. Chem. Biol.* **13**, 91–98 (2017).
- Wu, M., Xu, L. G., Li, X., Zhai, Z. & Shu, H. B. AMID, an apoptosis-inducing factor-homologous mitochondrial-associated protein, induces caspase-independent apoptosis. *J. Biol. Chem.* **277**, 25617–25623 (2002).
- Ingold, I. et al. Selenium utilization by GPX4 is required to prevent hydroperoxide-induced ferroptosis. *Cell* **172**, 409–422 (2018).
- Viswanathan, V. S. et al. Dependency of a therapy-resistant state of cancer cells on a lipid peroxidase pathway. *Nature* **547**, 453–457 (2017).
- Hangauer, M. J. et al. Drug-tolerant persister cancer cells are vulnerable to GPX4 inhibition. *Nature* **551**, 247–250 (2017).
- Tsoi, J. et al. Multi-stage differentiation defines melanoma subtypes with differential vulnerability to drug-induced iron-dependent oxidative stress. *Cancer Cell* **33**, 890–904 (2018).
- Angeli, J. P. F., Shah, R., Pratt, D. A. & Conrad, M. Ferroptosis inhibition: mechanisms and opportunities. *Trends Pharmacol. Sci.* **38**, 489–498 (2017).
- Horikoshi, N., Cong, J., Kley, N. & Shenk, T. Isolation of differentially expressed cDNAs from p53-dependent apoptotic cells: activation of the human homologue of the *Drosophila* peroxidasin gene. *Biochem. Biophys. Res. Commun.* **261**, 864–869 (1999).
- Bersuker, K. et al. The CoQ oxidoreductase FSP1 acts parallel to GPX4 to inhibit ferroptosis. *Nature* <https://doi.org/10.1038/s41586-019-1705-2> (2019).
- Seiler, A. et al. Glutathione peroxidase 4 senses and translates oxidative stress into 12/15-lipoxygenase dependent- and AIF-mediated cell death. *Cell Metab.* **8**, 237–248 (2008).
- Eisenhaber, F. et al. Prediction of lipid posttranslational modifications and localization signals from protein sequences: big-Π, NMT and PTS1. *Nucleic Acids Res.* **31**, 3631–3634 (2003).
- Borgese, N., Aggujaro, D., Carrera, P., Pietrini, G. & Bassetti, M. A role for N-myristoylation in protein targeting: NADH-cytochrome *b*<sub>5</sub> reductase requires myristic acid for association with outer mitochondrial but not ER membranes. *J. Cell Biol.* **135**, 1501–1513 (1996).
- Mounier, A. et al. Fragment-derived inhibitors of human N-myristoyltransferase block capsid assembly and replication of the common cold virus. *Nat. Chem.* **10**, 599–606 (2018).

23. Elguindy, M. M. & Nakamaru-Ogiso, E. Apoptosis-inducing factor (AIF) and its family member protein, AMID, are rotenone-sensitive NADH:ubiquinone oxidoreductases (NDH-2). *J. Biol. Chem.* **290**, 20815–20826 (2015).
24. Frei, B., Kim, M. C. & Ames, B. N. Ubiquinol-10 is an effective lipid-soluble antioxidant at physiological concentrations. *Proc. Natl Acad. Sci. USA* **87**, 4879–4883 (1990).
25. Haidasz, E. A., Van Kessel, A. T. & Pratt, D. A. A continuous visible light spectrophotometric approach to accurately determine the reactivity of radical-trapping antioxidants. *J. Org. Chem.* **81**, 737–744 (2016).
26. Niki, E. Mechanisms and dynamics of antioxidant action of ubiquinol. *Mol. Aspects Med.* **18**, 63–70 (1997).
27. Mannes, A. M., Seiler, A., Bosello, V., Maiorino, M. & Conrad, M. Cysteine mutant of mammalian GPx4 rescues cell death induced by disruption of the wild-type selenoenzyme. *FASEB J.* **25**, 2135–2144 (2011).
28. Shimada, K., Hayano, M., Pagano, N. C. & Stockwell, B. R. Cell-line selectivity improves the predictive power of pharmacogenomic analyses and helps identify NADPH as biomarker for ferroptosis sensitivity. *Cell Chem. Biol.* **23**, 225–235 (2016).
29. Shimada, K. et al. Global survey of cell death mechanisms reveals metabolic regulation of ferroptosis. *Nat. Chem. Biol.* **12**, 497–503 (2016).
30. Morré, D. J. & Morré, D. M. Non-mitochondrial coenzyme Q. *Biofactors* **37**, 355–360 (2011).
31. Nyquist, S. E., Barr, R. & Morré, D. J. Ubiquinone from rat liver Golgi apparatus fractions. *Biochim. Biophys. Acta* **208**, 532–534 (1970).
32. Rees, M. G. et al. Correlating chemical sensitivity and basal gene expression reveals mechanism of action. *Nat. Chem. Biol.* **12**, 109–116 (2016).
33. Seashore-Ludlow, B. et al. Harnessing connectivity in a large-scale small-molecule sensitivity dataset. *Cancer Discov.* **5**, 1210–1223 (2015).
34. Basu, A. et al. An interactive resource to identify cancer genetic and lineage dependencies targeted by small molecules. *Cell* **154**, 1151–1161 (2013).

**Publisher's note** Springer Nature remains neutral with regard to jurisdictional claims in published maps and institutional affiliations.

© The Author(s), under exclusive licence to Springer Nature Limited 2019

## Reporting summary

Further information on research design is available in the Nature Research Reporting Summary linked to this paper.

## Data availability

For immunoblot source data, see Supplementary Fig. 1. Source Data for Figs. 1–4 and Extended Data Figs. 1–6, 8, 9 are provided with the paper.

**Acknowledgements** This work is supported by the Junior Group Leader program of the Rudolf Virchow Center, University of Würzburg and Deutsche Forschungsgemeinschaft (DFG) FR 3746/3-1 to J.P.F.A., the DFG CO 291/5-2 and CO 291/7-1, the German Federal Ministry of Education and Research (BMBF) through the Joint Project Modelling ALS Disease In vitro (MAIV, 01EK1611B) and the VIP+ program NEUROPROTEKT (03VP04260), as well as the m<sup>4</sup> Award provided by the Bavarian Ministry of Economic Affairs, Regional Development and Energy (StMWi) to M.C., the Cancer Research UK (CRUK, grants C29637/A20183 and C29637/A21451) to E.W.T., the European Research Council (LipidArrays) to V.O., the Natural Sciences and Engineering Council of Canada and the Canada Foundation for Innovation to D.A.P. and PhD scholarship by DFG GRK2157 to A.K.

**Author contributions** M.C., J.P.F.A. and S.D. conceived the study and wrote the manuscript. M.A. and V.O. performed (oxi)lipidomics analysis and data interpretation. S.D., B.P., E.P., D.W., F.P.F., J.P.F.A., T.V., V.M., I.I., K.B., M. Sato, M.R., T.N.X.d.S. and M.C.d.S. performed in vitro experiments. R.S. and D.A.P. performed functional characterization of recombinant FSP1. S.D., F.P.F., D.A.P., J.P.F.A. and M.C. performed evaluation and interpretation of the in vitro data. M. Sattler, A.M. and G.M.P. expressed and purified recombinant FSP1. C.H.S. provided TNBC cell lines. A.F. and A. Schepers helped to generate the monoclonal antibodies. B.P. and J.W. carried out screening of FSP1 inhibitors and related structure–activity relationship studies. W.S. and A. Schulze performed liquid chromatography–mass spectrometry analysis of ubiquinone content. A.G.G. and E.W.T. studied myristoylation of FSP1. A.K., M. Sauer, F.P.F. and J.P.F.A. performed enhanced microscopy experiments. All authors read and agreed on the content of the paper.

**Competing interests** The authors declare no competing interests.

### Additional information

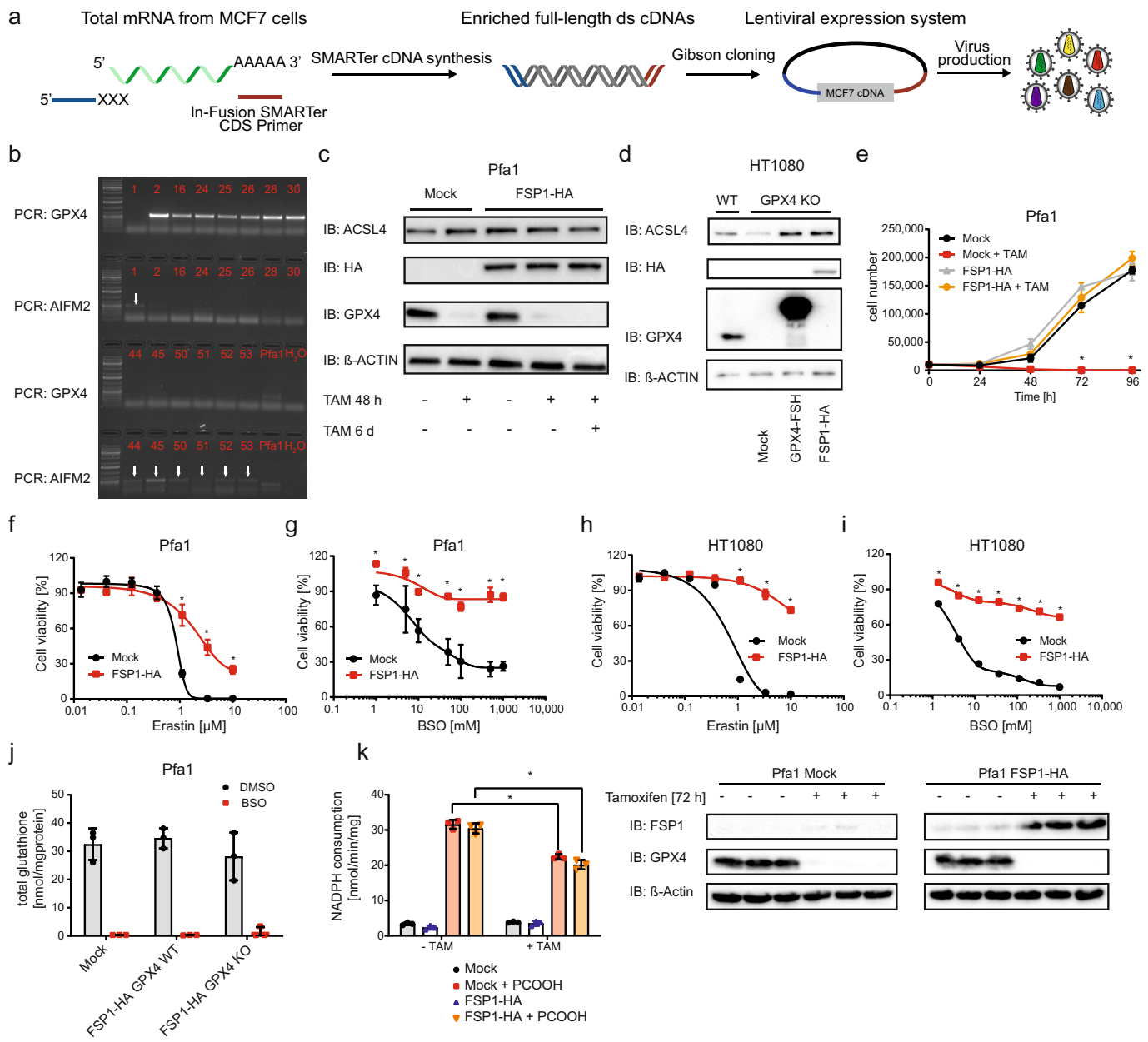
**Supplementary information** is available for this paper at <https://doi.org/10.1038/s41586-019-1707-0>.

**Correspondence and requests for materials** should be addressed to J.P.F.A. or M.C.

**Peer review information** *Nature* thanks Kivanc Birsoy, Navdeep S. Chandel and Brent R. Stockwell for their contribution to the peer review of this work.

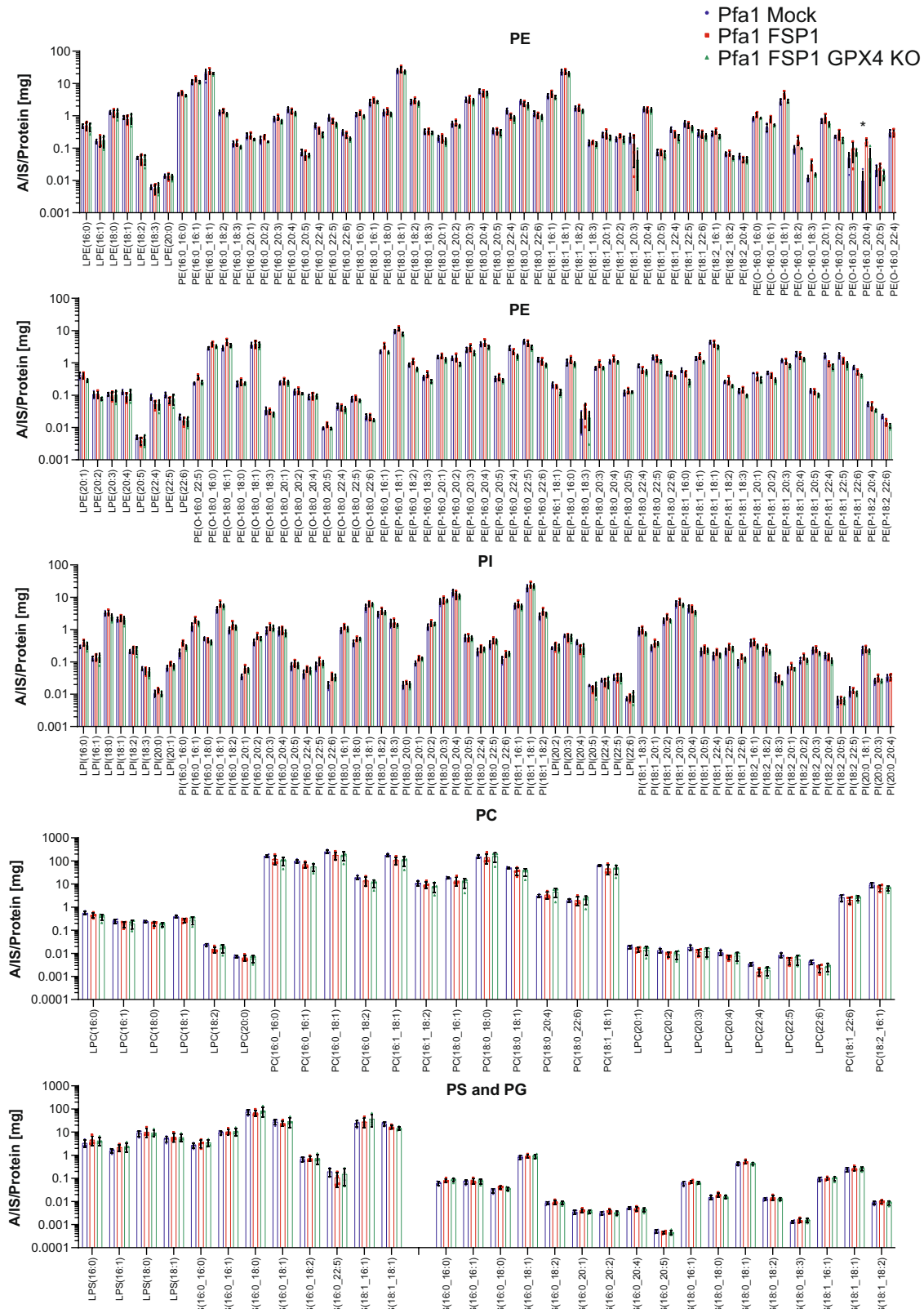
**Reprints and permissions information** is available at <http://www.nature.com/reprints>.

# Article



**Extended Data Fig. 1 | Identification and characterization of FSP1 as an anti-ferroptotic protein.** **a**, Schematic depicting the generation of a lentiviral cDNA-overexpression library using the total mRNA from MCF7 cells. **b**, Genomic PCRs of the 14 Pfa1 cell clones that remained clones after the removal of false-positive results using human-specific primers to amplify the human cDNAs of *GPX4* (571 bp) or *AIFM2* (524 bp). The clones 2, 16, 24, 25, 26, 28 and 30 showed positive PCR results for *GPX4* (571 bp). Clones 1, 44, 45, 50, 51, 52 and 53 were positive for *AIFM2* (524 bp) as indicated by the white arrows. Data are one of  $n=3$  independent experiments. **c**, Immunoblot analysis of ACSL4, HA, GPX4 and β-actin expression in Pfa1 cells stably expressing mock or FSP1-HA. *Gpx4* deletion was induced by the administration of TAM for the indicated time period. **d**, Immunoblot analysis of ACSL4, HA, GPX4 and β-actin expression in wild-type and *GPX4*-knockout HT1080 cells stably expressing mock, *GPX4*-FSH or FSP1-HA. **e**, Proliferation of mock and FSP1-HA Pfa1 cells treated with or without TAM. Cell numbers were assessed every 24 h using a Neubauer haemocytometer. Data are mean ± s.d. of  $n=3$  wells of a 24-well plate from one representative of two independent experiments. **f,g**, Dose-dependent toxicity of erasin (**f**) and L-buthionine sulfoximine (BSO; **g**), which is an inhibitor of γ-glutamyl-cysteine ligase, in Pfa1 cells expressing mock or

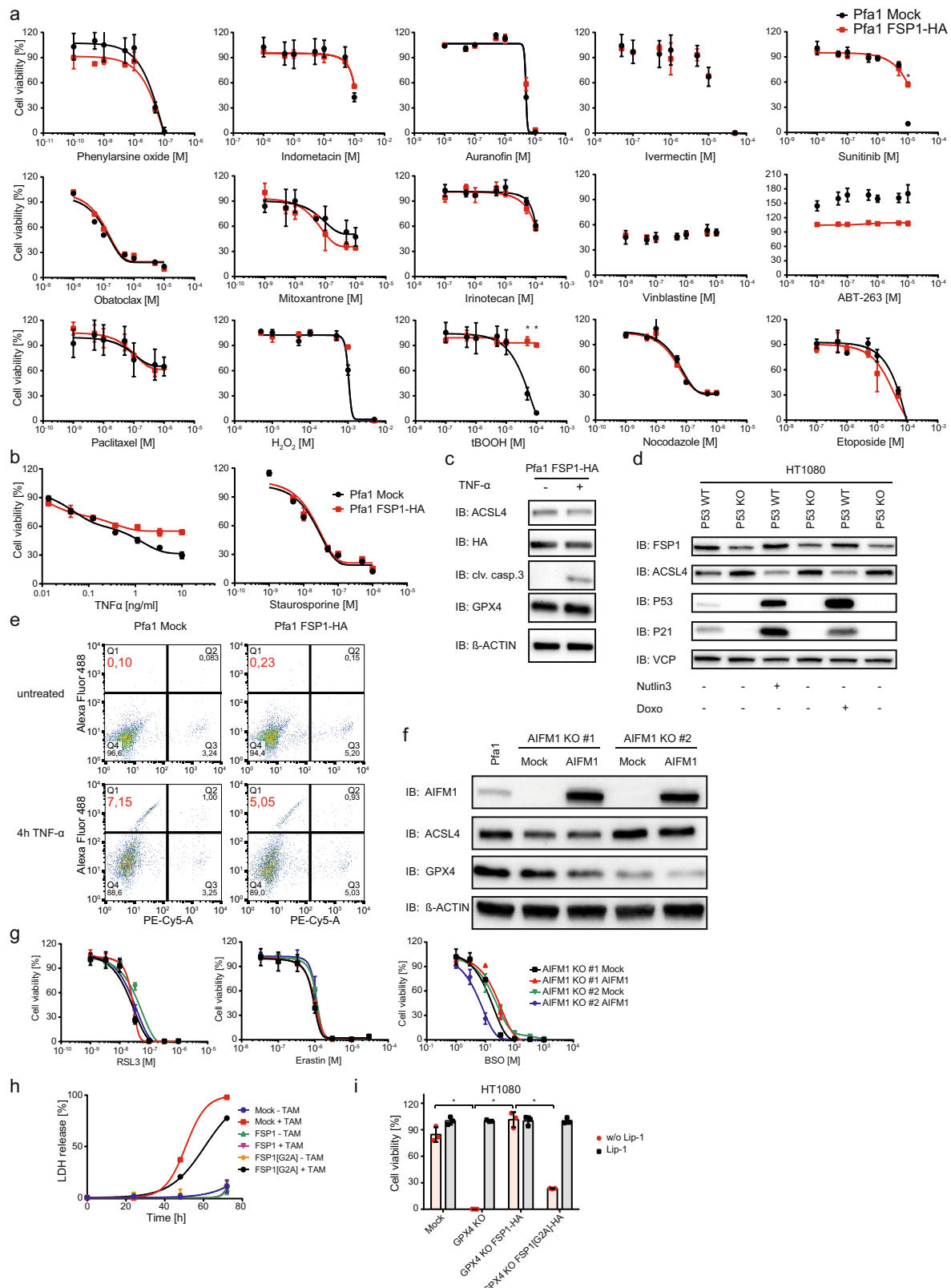
FSP1-HA. **h,i**, Dose-dependent toxicity of erasin (**h**) and BSO (**i**) in HT1080 cells expressing mock or FSP1-HA. Cell viability was assessed 48 h (**f,h**) or 72 h (**g,i**) after treatments using Aquabluer. Data are mean ± s.d. of  $n=3$  wells of a 96-well plate from one representative of three (**f-i**) independent experiments. \* $P<0.01$ ; two-way ANOVA. **j**, Measurement of total glutathione levels in Pfa1 mock, FSP1-expressing and FSP1-expressing *Gpx4*-knockout cells treated with or without BSO. Data are mean ± s.d. of  $n=3$  wells of a 96-well plate from one representative of three independent experiments. **k**, Left, determination of NADPH consumption by glutathione reductase as an indirect measure of the GPX4 activity. Phosphatidylcholine lipid hydroperoxide (PCOOH) was used as a GPX4-specific substrate. Right, cell lysates from mock and FSP1-HA Pfa1 cells treated with or without TAM for 48 h were used for the assay as shown by the immunoblot (FSP1, GPX4 and β-actin). FSP1 was detected using the polyclonal antibody (PA5-24562). Data are mean ± s.d. of  $n=3$  wells of a 6-well plate from one representative of three independent experiments. Immunoblot images (**c,d,k**) are cropped from the chemiluminescence signal files. For gel source data (**c,d,k**) showing the overlap of colorimetric and chemiluminescence signals, see Supplementary Fig. 1.



**Extended Data Fig. 2 | FSP1 expression does not change the phospholipid composition.** Lipidomic profile (only detectable phospholipid species of phosphatidylethanolamine (PE), phosphatidylcholine (PC), phosphatidylglycerol (PG), phosphatidylinositol (PI) and phosphatidylserine (PS), including plasmenyl (O) and plasmanyl (P) lipids) of mock, FSP1-HA and *Gpx4*-knockout FSP1-HA Pfa1 cells. Data are the mean values of the area of

analyte (A) over the internal standard (IS) per total protein (mg) of  $n=4$  replicates of one experiment performed independently three times.  $\log_{10}$ -transformation has been applied to better visualize and compare the abundance of the different phospholipid species in the samples. \* $P < 0.05$ ; multiple  $t$ -test with Sidak-Bonferroni correction for multiple comparisons.

# Article



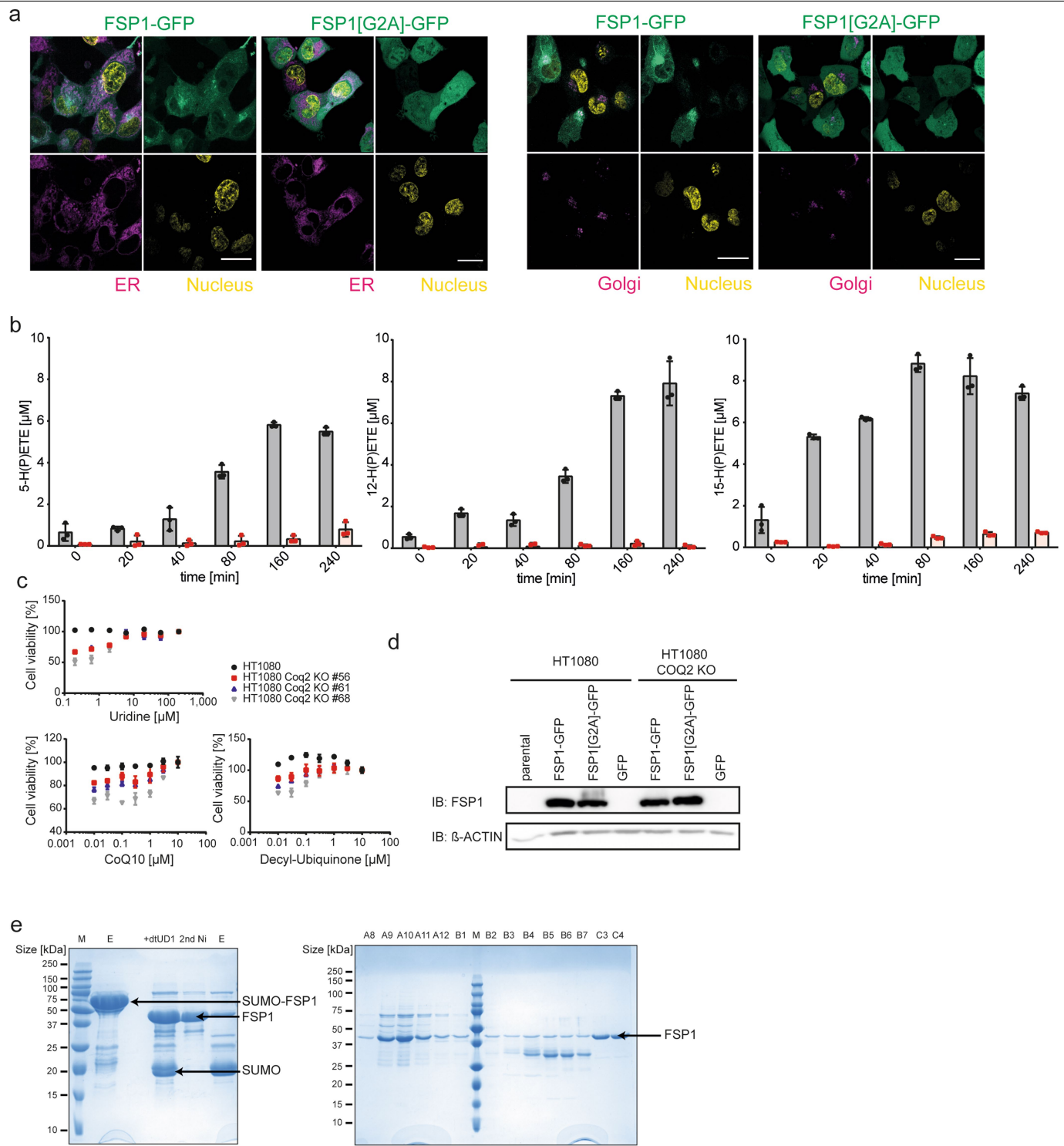
**Extended Data Fig. 3** | See next page for caption.

**Extended Data Fig. 3 | FSP1 is a highly specific anti-ferroptotic protein.**

**a**, Dose-dependent toxicity of phenylarsine oxide, indomethacin, auranofin, ivermectin, sunitinib, obatoclax, mitoxantrone, irinotecan, vinblastine, ABT-263, nocodazole, etoposide, paclitaxel, H<sub>2</sub>O<sub>2</sub> and tert-butyl hydroperoxide (tBOOH) of Pfa1 cells expressing mock or FSP1-HA. Cell viability was assessed 24 h after treatment using Aquabluer. **b**, Dose-dependent toxicity of TNF and staurosporine of mock and FSP1-HA-expressing Pfa1 cells. Cell viability was assessed 24 h after treatment using Aquabluer. **c**, Immunoblot analysis (ACSL4, HA, cleaved caspase 3 (clv. Casp3), GPX4 and β-actin) of Pfa1 FSP1-HA cells treated with or without TNF for 6 h. **d**, Immunoblot analysis of FSP1, ACSL4, p53, p21 and VCP expression in p53 (also known as TP53) wild-type and p53-knockout (CRISPR-CAS9-modified) HT1080 cell lines treated with the MDM2 (MDM2 proto-oncogene) inhibitor Nutlin3 or the cytostatic compound doxorubicin (Doxo). Expression of FSP1 was not altered by Nutlin3 or doxorubicin treatment, whereas the expression of p53 and p21 was strongly induced in HT1080 p53 wild-type cells. Data show one representative of  $n = 3$  independent experiments. **e**, Flow cytometry analysis of annexin V/propidium iodide staining in Pfa1 cells expressing mock or FSP1-HA treated with or without TNF for 4 h. No difference in the apoptotic activity was observed in cells as visualized in the Alexa Fluor 488/PE-Cy5 channels. Data show one

representative experiment of an experiment performed independently twice. **f**, Immunoblot analysis of AIFM1, ACSL4, GPX4 and β-actin in two different Pfa1 *Aifm1*-knockout cell clones overexpressing mock or AIFM1. Data show one representative of  $n = 3$  independent experiments. **g**, Dose-dependent toxicity of RSL3, erastin and BSO in *Aifm1*-knockout Pfa1 cell clones (1 and 2) overexpressing mock or AIFM1. AIFM1 expression does not affect ferroptosis sensitivity. Data are the mean of  $n = 3$  replicates of a representative experiment performed independently three times. **h**, Time-dependent lactate dehydrogenase (LDH) release of Pfa1 cells stably expressing mock, FSP1-HA or FSP1(G2A) treated with TAM to induce GPX4 loss. Supernatants were collected from 6-well plates at different time points after TAM induction and assayed for lactate dehydrogenase content in a 96-well plate. **i**, Wild-type and GPX4-knockout HT1080 cells overexpressing mock, hGPX4-FSH, FSP1-HA or FSP1(G2A)-HA treated with and without 200 nM Lip-1. Cell viability was assessed after 72 h using Aquabluer. Data are the mean ± s.d. of  $n = 3$  wells of a 96-well plate from one representative of three independent experiments (**a, b, g-i**); \* $P < 0.01$ ; two-way ANOVA. Immunoblot images (**c, d, f**) are cropped from the chemiluminescence signal files. For gel source data (**c, d, f**) showing the overlap of colorimetric and chemiluminescence signals, see Supplementary Fig. 1.

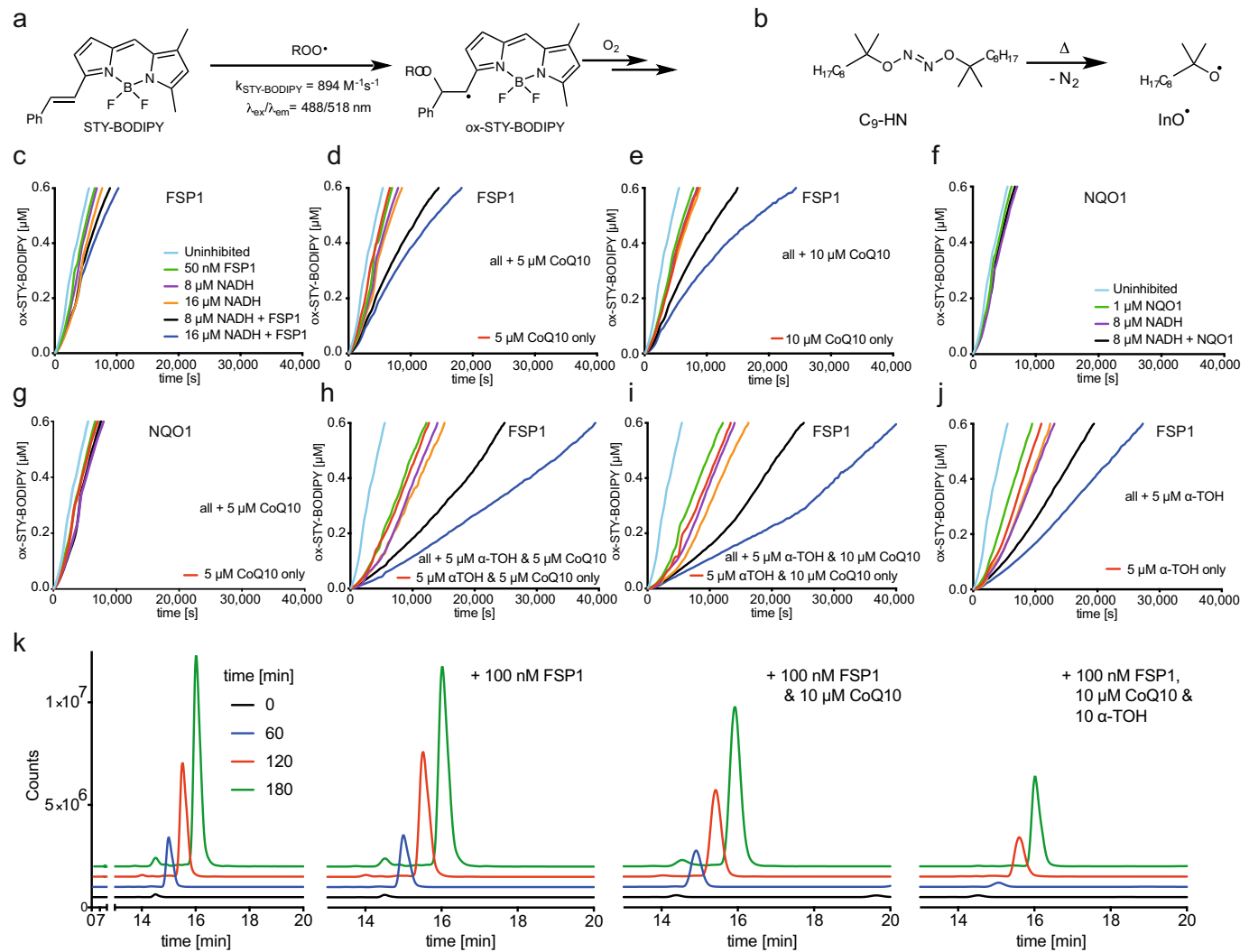
# Article



**Extended Data Fig. 4** | See next page for caption.

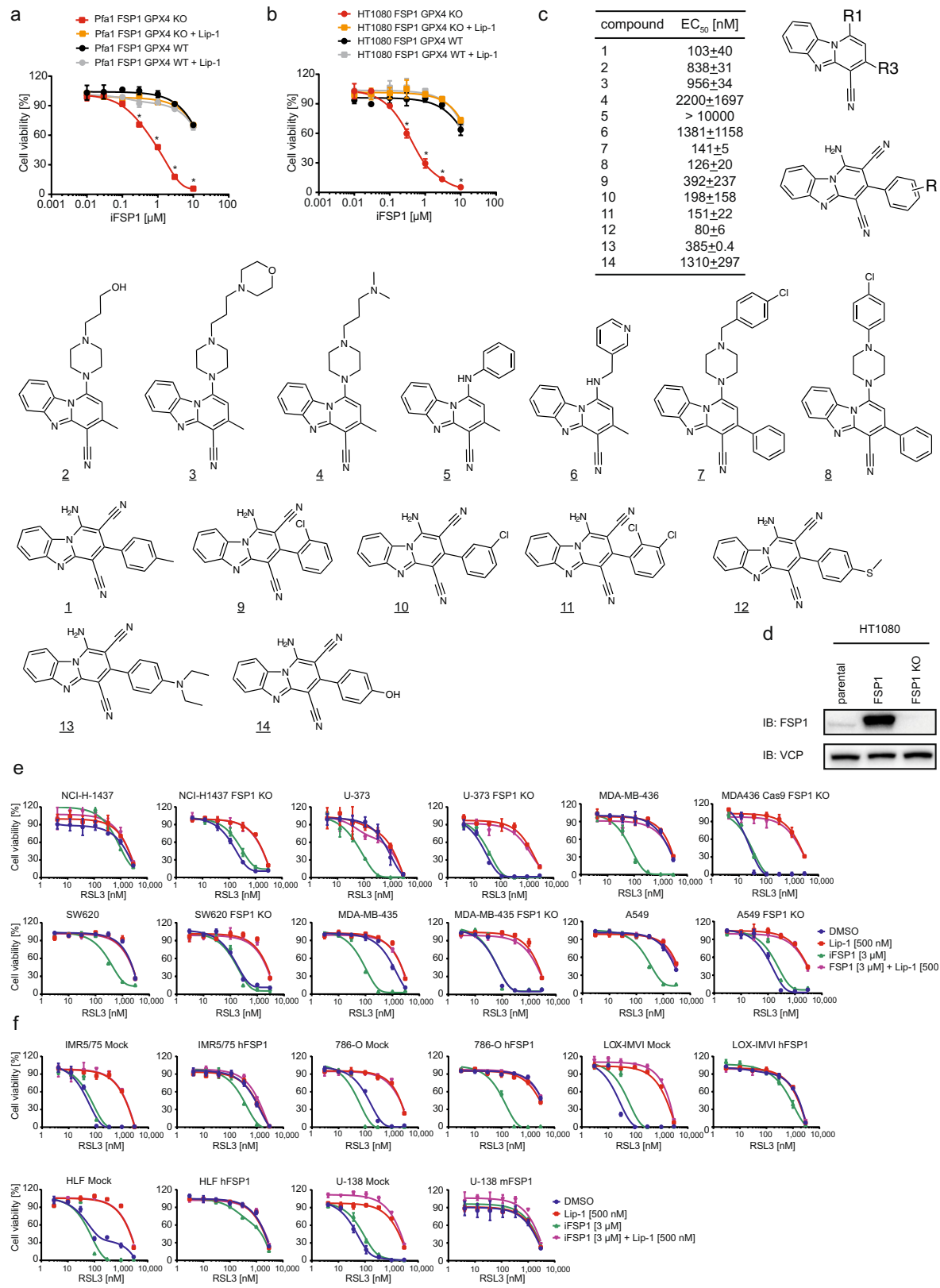
**Extended Data Fig. 4 | FSP1 protects against unrestrained lipid peroxidation in a COQ2-dependent manner.** **a**, Enhanced resolution confocal microscopy images demonstrating different localizations of FSP1–GFP and the FSP1(G2A)–GFP mutant in HT1080 cells. DAPI (yellow), GFP (green), endoplasmic reticulum or Golgi tracker (magenta). Scale bars, 20 nm. Data show one representative of  $n = 3$  independently performed experiments. **b**, Formation of 5-hydro(pero)xyeicosatetraenoic acid (5-H(P)ETE) (multiple reaction monitoring (MRM): 319 → 115), 12-H(P)ETE (MRM: 319 → 179) and 15-H(P)ETE (MRM: 319 → 219) in either mock (black) or FSP1–HA-overexpressing (red) Pfa1 cells treated with 0.2 μM RSL3 and 40 μM arachidonic acid. Hydroperoxides were analysed as their alcohols following reduction with PPh<sub>3</sub> (triphenylphosphane) in methanol. Data are the mean of biological triplicates from one representative of  $n = 3$  independently performed experiments. **c**, Dose-dependent rescue of three independent COQ2-knockout HT1080 cell clones (56, 61 and 68) by supplementation of the cell culture medium with uridine, CoQ<sub>10</sub> or decyl-ubiquinone. Cell viability was assed using the Aquabluer assay 48 h after treatment. Data are mean ± s.d. of  $n = 3$  wells of a

96-well plate performed once. **d**, Immunoblot analysis of FSP1 and β-actin in HT1080 parental (left) and HT1080 COQ2-knockout (56) (right) cells overexpressing FSP1–GFP, FSP1(G2A)–GFP or GFP. Immunoblot images are cropped from the chemiluminescence signal files. For gel source data showing the uncropped chemiluminescence signals, see Supplementary Fig. 1. **e**, SDS gels showing the different purification steps of recombinant FSP1 from bacterial cell lysates. Left, SDS gel of protein extracts after initial nickel affinity chromatography (E1), the SUMO-tag was cleaved in the eluate by addition of the SUMO protease (dtUD1) and a second round of nickel affinity chromatography was performed to remove the cleaved SUMO-tag as well as uncleaved SUMO–FSP1 and SUMO protease (E2). The flow-through fraction was collected (second nickel). The SUMO–FSP1 fusion protein is visible around 55 kDa and FSP1 at 40.5 kDa. Right, SDS gel showing different fractions containing FSP1 40.5 kDa (A8–A12, B1–B7 and C3–C4) from size-exclusion chromatography of FSP1 after the second nickel-affinity chromatography. Fractions C3 and C4 were used for subsequent assays. One representative of at least three independent experiments.



**Extended Data Fig. 5 | FSP1 protects against lipid peroxidation by reducing radical-trapping antioxidants.** **a, b**, Co-autoxidations of STY-BODIPY (1  $\mu\text{M}$ ) (a) and the polyunsaturated lipids of chicken egg phosphatidylcholine liposomes (1 mM). The increase in fluorescence of oxidized STY-BODIPY is monitored over the course of the autoxidation, which is initiated using  $\text{C}_9\text{-HN}$  (0.2 mM) (b). **c**, Representative autoxidations inhibited by 50 nM FSP1 (green), 8  $\mu\text{M}$  NADH (purple), 16  $\mu\text{M}$  NADH (orange), 50 nM FSP1 and 8  $\mu\text{M}$  NADH (black) or 50 nM FSP1 and 16  $\mu\text{M}$  NADH (blue) (c). **d–j**, Analogous representative of inhibited autoxidations to which  $\text{CoQ}_{10}$  (d, e),  $\alpha$ -tocopherol ( $\alpha$ -tocopherol) and

$\text{CoQ}_{10}$  (h, i), or  $\alpha$ -tocopherol (j) was added. **f, g**, Recombinant NQO1 failed to suppress autoxidations in a similar manner compared to FSP1 (f, g). **k**, 1-Palmitoyl-2-linoleoyl-phosphatidylcholine hydroperoxide (PLPC-OOH) produced from the autoxidation of soy lecithin liposomes (13.3 mM), inhibited by FSP1 alone, or in the presence of either 10  $\mu\text{M}$   $\text{CoQ}_{10}$  or 10  $\mu\text{M}$   $\alpha$ -tocopherol and 10  $\mu\text{M}$   $\text{CoQ}_{10}$ . PLPC-OOH was measured 0, 60, 120 and 180 min after autoxidation was induced using liquid chromatography–mass spectrometry (MRM: 790  $\rightarrow$  184). Data show one of  $n=3$  representative experiments.

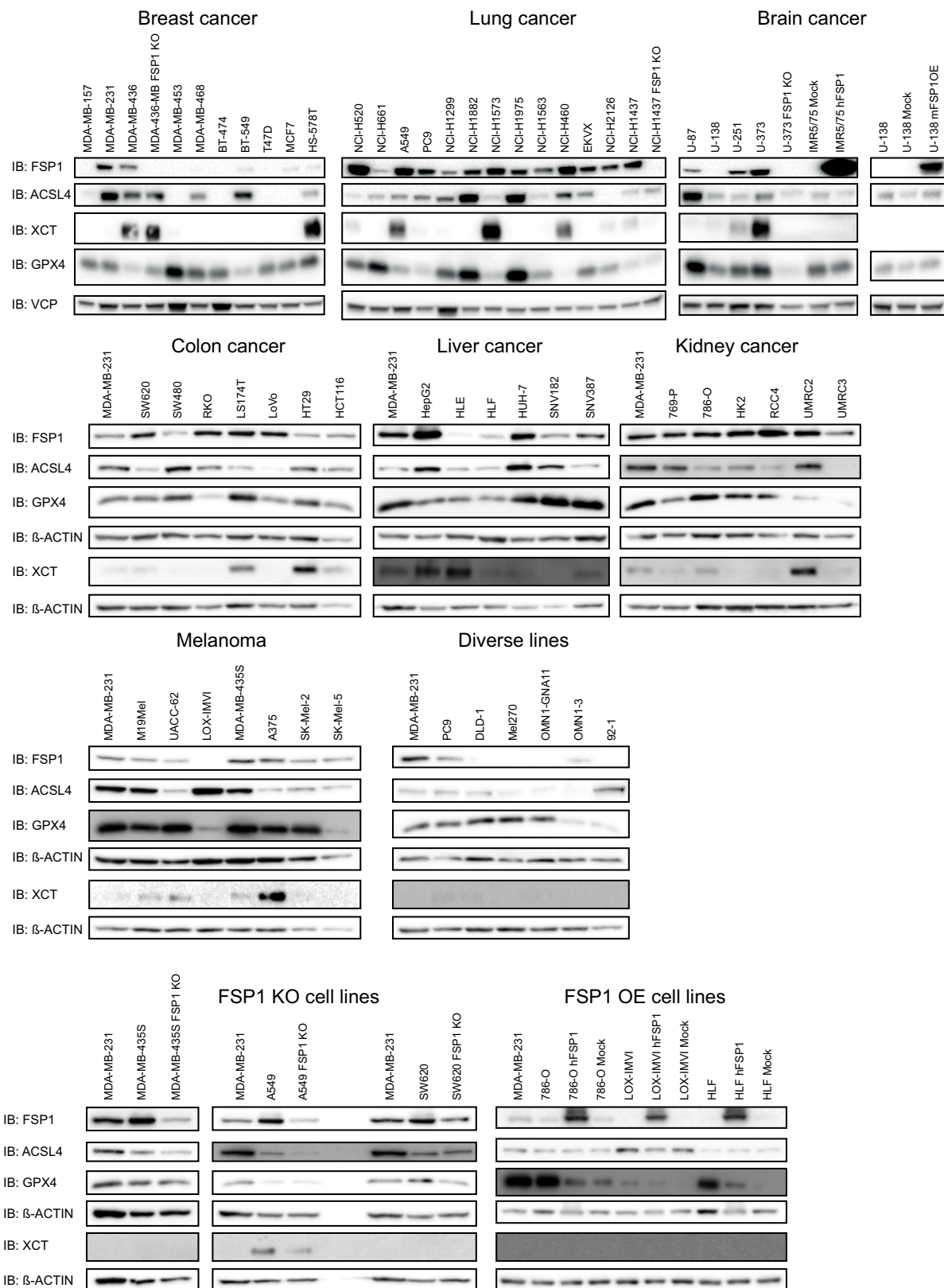


**Extended Data Fig. 6** | See next page for caption.

# Article

**Extended Data Fig. 6 | Development of FSP1-specific inhibitors as ferroptosis sensitizer.** **a, b**, Dose-dependent toxicity of iFSP1 in FSP1-overexpressing cells (Pfa1 (**a**); HT1080 (**b**)) with or without *GPX4* loss. Treatment with the ferroptosis inhibitor Lip-1 (150 nM) protected *GPX4*-knockout cells from iFSP1-induced ferroptosis. iFSP1 is only toxic to cells that depend solely (no *GPX4* expression detectable) on FSP1 function. **c**, Efficacy of iFSP1 and structurally related analogues; half-maximal effective concentration ( $EC_{50}$ ) values (mean  $\pm$  s.d.) of iFSP1 (**1**) and its derivatives (**2–14**) calculated from experiments performed at least twice in triplicate are shown in the table with the corresponding chemical structures depicted below. Based on commercially available analogues a preliminary structure–activity relationship study revealed that substitution of the amino position (R1, R2) showed broad tolerability of aliphatic groups and that lipophilic substituents of the phenyl group at the 3 position (R3) in the *ortho* and *meta* positions were well tolerated. **d**, Immunoblot analysis of FSP1 and VCP in parental as well as HT1080 FSP1-overexpressing and *FSP1*-knockout HT1080 cells. An in-house-

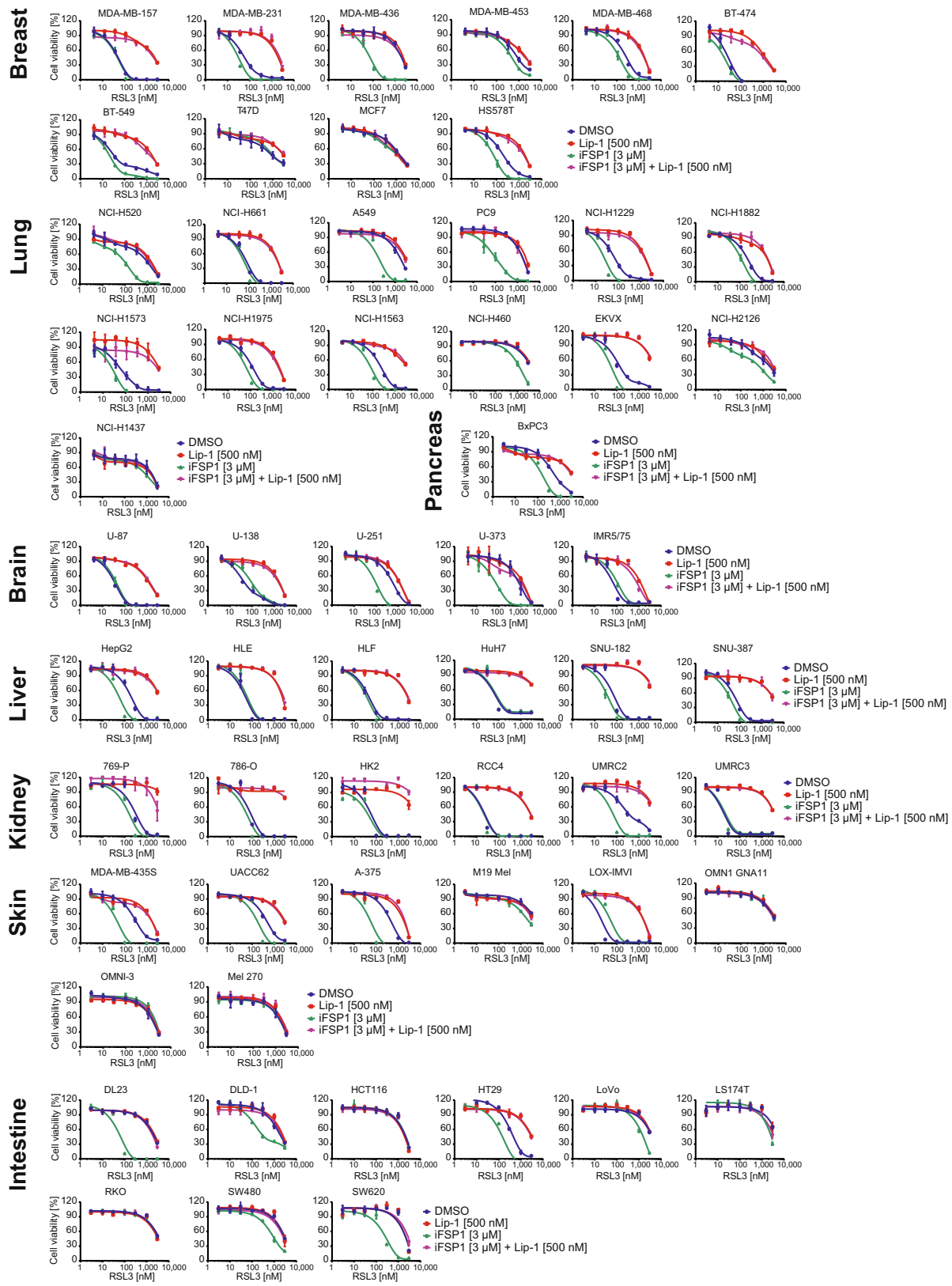
generated monoclonal antibody against human FSP1 was used. Immunoblot images are cropped from the chemiluminescence signal files. For gel source data showing the overlap of colorimetric and chemiluminescence signals, see Supplementary Fig. 1. **e**, Dose-dependent toxicity of RSL3 in a panel of genetically engineered (*FSP1*-knockout) human cancer cell lines (NCI-H1437, NCI-H1437 *FSP1* KO, U-373, U-373 *FSP1* KO, MDA-MB-436, MDA-MB-436 *FSP1* KO, SW620, SW620 *FSP1* KO, MDA-MB-435S, MDA-MB-435S *FSP1* KO, A549 and A549 *FSP1* KO) treated with or without FSP1 inhibitor (iFSP1) and Lip-1. **f**, Dose-dependent toxicity of RSL3 in a panel of genetically modified (mouse (mFSP1) and human (hFSP1) FSP1 overexpression) human cancer cell lines (IMR5/75 mock, IMR5/75 hFSP1, 786-O mock, 786-O hFSP1, LOX-IMVI mock, LOX-IMVI hFSP1, HLF mock, HLF hFSP1, U-138 mock and U-138 mFSP1) treated with or without iFSP1 and Lip-1. Data show the mean  $\pm$  s.d. of  $n=3$  wells of a 96-well plate from one representative of three (**a–c**) or two (**e, f**) independent experiments; \* $P<0.0001$ ; two-way ANOVA.



#### Extended Data Fig. 7 | FSP1 is expressed in a wide range of cancer cell lines.

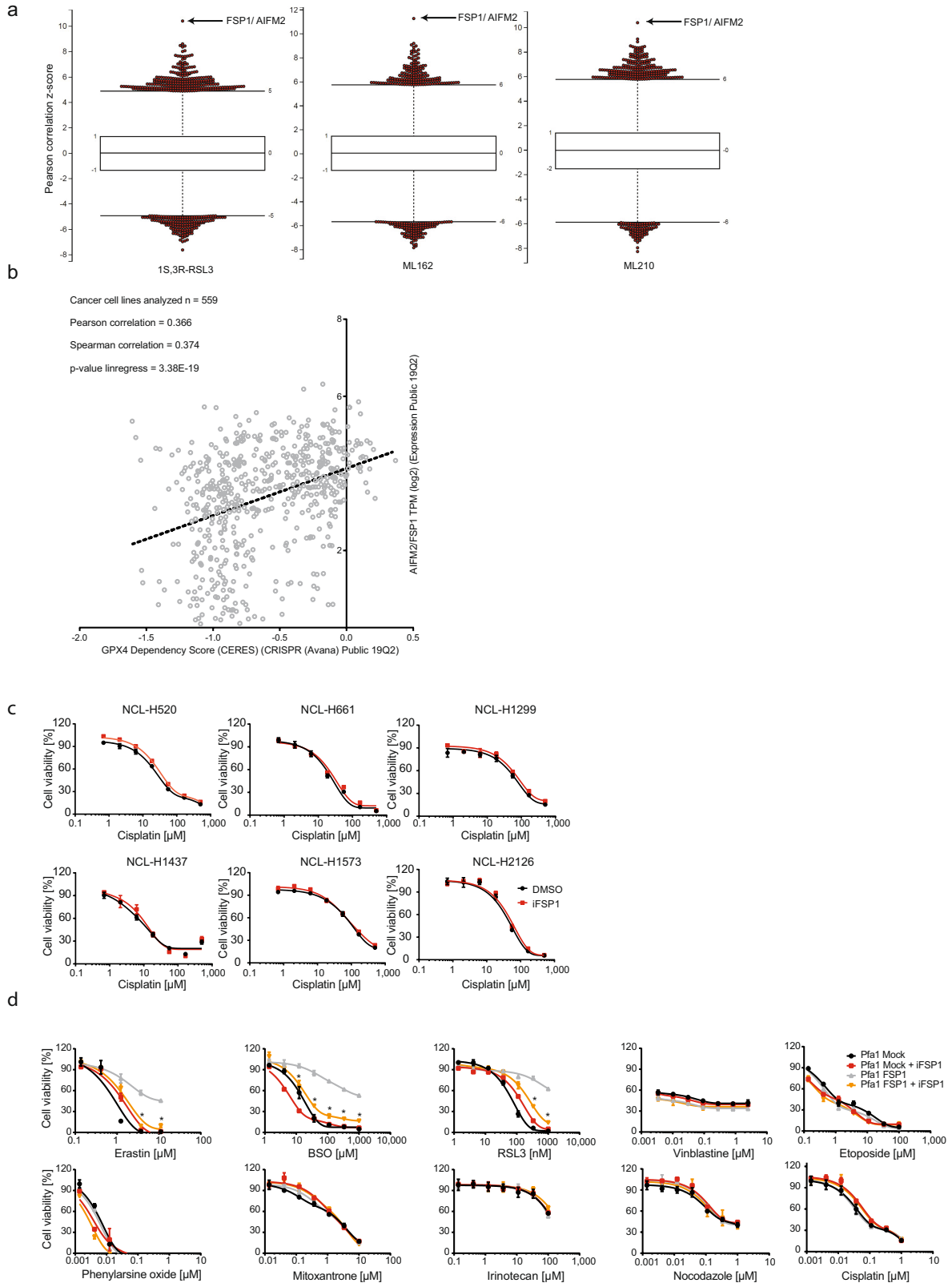
**a**, Immunoblot analysis of the expression of key ferroptosis players including ACSL4, FSP1, GPX4 and XCT (SLC7A11) in a panel of cancer cell lines from different origins. In addition, genetically modified cancer cell lines in which FSP1 is knocked out (MDA-436-MB *FSP1* KO, NCI-H1437 *FSP1* KO, U-373 *FSP1* KO, MDA-MB-435S *FSP1* KO, A549 *FSP1* KO and SW620 *FSP1* KO) as well as cell lines with lentiviral overexpression of FSP1 (IMR5/75 hFSP1, 786-O hFSP1, LOX-IMVI

hFSP1 and HLF hFSP1) are shown. VCP or  $\beta$ -actin served as loading control. MDA-MB-231 was used as reference to compare expression levels in between independent blots. Data show one representative of two independent experiments. Immunoblot images are cropped from the chemiluminescence signal files. For gel source data showing the overlap of colorimetric and chemiluminescence signals, see Supplementary Fig. 1.



**Extended Data Fig. 8 | iFSP1 sensitizes cancer cell lines from different origins to RSL3-induced ferroptosis.** Dose-dependent toxicity of RSL3 in a panel of human cancer cell lines from different origins (breast, lung, pancreas,

brain, liver, kidney, skin and intestine) treated with or without iFSP1 and Lip-1. Data are the mean  $\pm$  s.d. of  $n=3$  wells of a 96-well plate from one representative of two independent experiments.



**Extended Data Fig. 9** | See next page for caption.

## Article

### Extended Data Fig. 9 | FSP1 expression directly correlates with resistance to ferroptosis and its inhibition selectively sensitizes cells to ferroptosis.

**a**, Correlation of a panel of 860 cancer cell lines<sup>32–34</sup>. The sensitivity to RSL3, ML162 and ML210 was correlated with gene expression. Genes were plotted according to their Pearson correlation score. *FSP1* was the highest ranking gene that correlated with resistance to RSL3 ( $P=0.392$ ), ML162 ( $P=0.424$ ) and ML210 ( $P=0.398$ ). **b**, Dot plot depicting the correlation of the dependency of a cell on *GPX4* (CERES score of -1 means full dependency based on CRISPR–Cas9 knockout screen) and the expression level of *FSP1* in a panel of 559 different cancer cell lines (DepMap; <https://depmap.org/portal/>). Cell lines with high expression of *FSP1* were found to be less dependent on *GPX4* (Pearson

correlation score of 0.366,  $P=3.38 \times 10^{-19}$ ). **c**, Dose-dependent toxicity of RSL3 in a panel of human lung cancer cells (NCI-H1437, NCI-H1299, NCI-H1573, NCI-H2126, NCI-H520 and NCI-H661) treated with or without the FSP1 inhibitor iFSP1 (5  $\mu$ M). Co-treatment of RSL3 and iFSP1 increased the ferroptotic response of all cell lines except in NCI-H1437 cells. **d**, Dose-dependent toxicity of different cytotoxic compounds (erastin, BSO, RSL3, vinblastine, etoposide, phenylarsine oxide (PAO), mitoxantrone, irinotecan, nocodazole and cisplatin) in Pfa1 mock and FSP1-overexpressing cells treated with or without iFSP1. The protective effect of FSP1 overexpression is lost upon iFSP1 (5  $\mu$ M) treatment. Data are the mean  $\pm$  s.d. of  $n=3$  wells of a 96-well plate from one representative of two independent experiments (**c, d**).

## Reporting Summary

Nature Research wishes to improve the reproducibility of the work that we publish. This form provides structure for consistency and transparency in reporting. For further information on Nature Research policies, see [Authors & Referees](#) and the [Editorial Policy Checklist](#).

### Statistics

For all statistical analyses, confirm that the following items are present in the figure legend, table legend, main text, or Methods section.

n/a Confirmed

- The exact sample size ( $n$ ) for each experimental group/condition, given as a discrete number and unit of measurement
- A statement on whether measurements were taken from distinct samples or whether the same sample was measured repeatedly
- The statistical test(s) used AND whether they are one- or two-sided  
*Only common tests should be described solely by name; describe more complex techniques in the Methods section.*
- A description of all covariates tested
- A description of any assumptions or corrections, such as tests of normality and adjustment for multiple comparisons
- A full description of the statistical parameters including central tendency (e.g. means) or other basic estimates (e.g. regression coefficient) AND variation (e.g. standard deviation) or associated estimates of uncertainty (e.g. confidence intervals)
- For null hypothesis testing, the test statistic (e.g.  $F$ ,  $t$ ,  $r$ ) with confidence intervals, effect sizes, degrees of freedom and  $P$  value noted  
*Give  $P$  values as exact values whenever suitable.*
- For Bayesian analysis, information on the choice of priors and Markov chain Monte Carlo settings
- For hierarchical and complex designs, identification of the appropriate level for tests and full reporting of outcomes
- Estimates of effect sizes (e.g. Cohen's  $d$ , Pearson's  $r$ ), indicating how they were calculated

*Our web collection on [statistics for biologists](#) contains articles on many of the points above.*

### Software and code

Policy information about [availability of computer code](#)

Data collection

FlowJo software, TraceFinder software, VisiView imaging software, Image Lab 5.1 Software, Softmax Pro 6.2.1 Software, BD FACSDiva v6.1.3, cSeries Capture Software, Version 1.9.7.0802 (2017, Azure Biosystems), CorelDraw X8 Version 18.0.0.448 (2016 Corel Corporation), SparkControl V2.1 (TEcan), MultiQuant 3.0.2 Software.

Data analysis

Microsoft Excel 2016 MSO (16.0.4266.1001), Graph Pad Prism 6 (Version 6.07), Graph Pad Prism 8 (Version 8.1.0), RStudio Version 1.1.463, Analyst® 1.7, were used for data analysis.

For manuscripts utilizing custom algorithms or software that are central to the research but not yet described in published literature, software must be made available to editors/reviewers. We strongly encourage code deposition in a community repository (e.g. GitHub). See the Nature Research [guidelines for submitting code & software](#) for further information.

### Data

Policy information about [availability of data](#)

All manuscripts must include a [data availability statement](#). This statement should provide the following information, where applicable:

- Accession codes, unique identifiers, or web links for publicly available datasets
- A list of figures that have associated raw data
- A description of any restrictions on data availability

The datasets generated during and/or analysed during the current study are available from the corresponding author on reasonable request.

# Field-specific reporting

Please select the one below that is the best fit for your research. If you are not sure, read the appropriate sections before making your selection.

Life sciences

Behavioural & social sciences

Ecological, evolutionary & environmental sciences

For a reference copy of the document with all sections, see [nature.com/documents/nr-reporting-summary-flat.pdf](http://nature.com/documents/nr-reporting-summary-flat.pdf)

## Life sciences study design

All studies must disclose on these points even when the disclosure is negative.

Sample size	No sample size calculation was performed. Preliminary cell viability experiments showed small variations between biological replicates, so we chose $n \geq 3$ for reproducibility. For the determination of phospholipid composition we chose $n \geq 4$ according to our experience in previous experiments (small variation between biological replicates).
Data exclusions	In very rare cases single values of biological triplicates were excluded from the analysis due to cell clumps/ uneven plating.
Replication	All attempts to replicate experiments were successful, accounting for the robustness of the results. To guarantee reliable replication of our results we pretested all used sera for their suitability for ferroptosis research. It is known that differing vitamin E and selenium concentrations in different sera batches profoundly impact on the outcome of ferroptosis inducing/inhibiting conditions.
Randomization	Not applicable as no animal studies were performed.
Blinding	Blinding was not required for cell viability measurements. For the determination of phospholipid composition the investigator performing the MS analysis and quantification was blinded.

## Reporting for specific materials, systems and methods

We require information from authors about some types of materials, experimental systems and methods used in many studies. Here, indicate whether each material, system or method listed is relevant to your study. If you are not sure if a list item applies to your research, read the appropriate section before selecting a response.

### Materials & experimental systems

n/a	Involved in the study
<input type="checkbox"/>	<input checked="" type="checkbox"/> Antibodies
<input type="checkbox"/>	<input checked="" type="checkbox"/> Eukaryotic cell lines
<input checked="" type="checkbox"/>	<input type="checkbox"/> Palaeontology
<input checked="" type="checkbox"/>	<input type="checkbox"/> Animals and other organisms
<input checked="" type="checkbox"/>	<input type="checkbox"/> Human research participants
<input checked="" type="checkbox"/>	<input type="checkbox"/> Clinical data

### Methods

n/a	Involved in the study
<input checked="" type="checkbox"/>	<input type="checkbox"/> ChIP-seq
<input type="checkbox"/>	<input checked="" type="checkbox"/> Flow cytometry
<input checked="" type="checkbox"/>	<input type="checkbox"/> MRI-based neuroimaging

## Antibodies

### Antibodies used

Antibodies against GPX4 (1:1000; no. ab125066, Abcam), ACSL4 (1:200; no. sc-271800, Santa Cruz),  $\beta$ -ACTIN (1:10000; no. A5441, Sigma), VCP (1:2000; ab11433, Abcam), AIFM2 (1:1000; PA5-24562, Thermo, Extended Data Fig. 1e), AIFM2 (1:10; Rat IgG2a monoclonal antibody raised against recombinant human AIFM2 protein, clone 6D8-11, developed in this study), XCT (1:10; Rat IgG2a monoclonal antibody raised against a N-terminal peptide of hXCT, clone 3A12-1-1, developed in-house), P53 (1:1000; p53 Antibody #9282, Cell Signaling), P21 (1:1000; p21 Waf1/Cip1 (12D1) Rabbit mAb #2947, Cell Signaling), cleaved caspase 3 (1:1000; cleaved caspase3 antibody (Asp175) #9661, Cell Signaling), HA tag (Rat IgG1 Anti-HA High affinity 3F10, Roche), ARL1 (1:500, no. 16012-1-AP, Proteintech) were used in this study.

### Validation

Antibody against GPX4 (no. ab125066) was validated for westernblotting in a previous publication (PMID: 25402683). Antibody against ACSL4 (no. sc-271800) was validated for westernblotting in a previous publication (PMID: 27842070). Antibody against  $\beta$ -ACTIN (A5441) was validated as loading control for westernblotting in a previous publication (PMID 15809369). Antibody against VCP (ab11433) has been validated as loading control in westernblotting in a previous publication (PMID: 19139805). Antibody against AIFM2 (PA5-24562) has been validated for westernblotting in this study in Extended Data Fig. 1e. Antibody against AIFM2 (clone 6D8-11, developed in this study) has been validated for westernblotting in this study Extended Data Fig. 4d. Antibody against XCT (clone 3A12-1-1, developed in this study) has been validated for westernblotting in this study Fig. 4a. P53 antibody (#9282) recognizes endogenous levels of P53 stated on by cell signaling website. P21 antibody (p21 Waf1/Cip1 (12D1) Rabbit mAb #2947) specificity validated on cell signaling website. Cleaved caspase 3 antibody (Antibody #9661) specificity validated on cell signaling website.

Antibody against HA tag (clone 3F10) was validated on the manufacturer's website.  
ARL1 antibody (no. 16012-1-AP) was validated on the manufacturer's website.

## Eukaryotic cell lines

Policy information about [cell lines](#)

Cell line source(s)

4-hydroxytamoxifen (TAM)-inducible Gpx4-/- murine immortalized fibroblasts (Pfa1) were reported previously (PMID: 18762024). Human fibrosarcoma (HT1080) cells, human hepatocellular carcinoma (HepG2, HLE, HLF, HUH-7, SNV182, SNV387 (HLE, HLF, HUH-7, SNV182 and SNV387 were all kind gifts from Prof. Martin Eilers, Würzburg University), human lung cancer cells (NCI-H1299, NCI-H1437, NCI-1882, NCI-H1563, NCI-H1573, NCI-H1975, NCI-H2126, NCI-H520, NCI-H661, A549, PC9, EKX, NCI-H460), human glioblastoma cells (U-87 MG, U-251 MG, U-138 MG, U-373 MG), human neuroblastoma cells (IMR5/75 (kind gift from Dr. Frank Westermann, DKFZ Heidelberg)), human breast cancer cells (MDA-MB-157, MDA-MB-231, MDA-MB-436, MDA-MB-453, MDA-MB-468, BT-474, BT-549, MCF7, T-47D, HS-578T), human colon cancer cells (SW620, SW480, RKO, LS174T, LoVo, HT29, HCT116, DLD-1), human kidney cancer cells (769-P, 786-O, LOX-IMVI, HK2, RCC4, UMRC2, UMRC3, human melanoma and uveal melanoma (M19Mel, UACC-62, LOX-IMVI, MDA-MB-435, A375, SK-Mel-2, SK-Mel-5, Mel270, OMN1-GNA11, OMN1-3 and 92-1 were all kind gifts from Prof. Svenja Meierjohann, Würzburg University) were purchased from ATCC unless stated otherwise and cultured according to ATCC guidelines. All cells were regularly tested for mycoplasma contamination.

Authentication

Non of the cell lines used were authenticated.

Mycoplasma contamination

All cell lines were tested negative for mycoplasma contamination.

Commonly misidentified lines  
(See [ICLAC](#) register)

MDA-MB-435 (SAMN03151832), U-373 MG (SAMN03151977)

## Flow Cytometry

### Plots

Confirm that:

- The axis labels state the marker and fluorochrome used (e.g. CD4-FITC).
- The axis scales are clearly visible. Include numbers along axes only for bottom left plot of group (a 'group' is an analysis of identical markers).
- All plots are contour plots with outliers or pseudocolor plots.
- A numerical value for number of cells or percentage (with statistics) is provided.

### Methodology

Sample preparation

Determination of apoptosis using AnnexinV/PI staining. 200,000 Pfa1 p442-Mock and Pfa1 p442-FSP1 cells were seeded on each well of a 6-well plate. On the next day, cells were treated with TNF $\alpha$  (10 ng/mL) for 4 h and stained according to the manufacturers protocol (eBioscience™ Annexin V Apoptosis Detection Kit FITC). Subsequently, they were analyzed on a BD FACSCANTO II instrument using the AlexaFluor 488 filter for the Fit-C labeled AnnexinV antibody and the PE-Cy5 filter for PI staining.

Assessment of lipid peroxidation using C11-BODIPY (581/591). 150,000 cells per well were seeded on 6-well dishes (Nunc) one day prior to the experiment. On the next day, cells were treated with the indicated concentration of (1S, 3R)-RSL3 to induce ferroptosis. Cells were incubated with C11-BODIPY (581/591) (1  $\mu$ M) for 30 min at 37°C before they were harvested by trypsinisation. Subsequently, cells were resuspended in 500  $\mu$ L of fresh PBS (DPBS, Gibco) strained through a 35  $\mu$ M cell strainer (Falcon tube with cell strainer CAP) and analyzed using the 488-nm laser of flow cytometer (FACS Canto II, BD Biosciences) for excitation. Data was collected from the FL1 detector (C11-BODIPY) with a 502LP and 530/30 BP filter. At least 10,000 events were analyzed per sample. Data was analyzed using FlowJo Software.

Pfa1\_Cas9 cells were used to generate Pfa1 AIFM1 KO cells by lentiviral infection with ecotropic pseudotyped particles containing the desired sgRNA expressing plasmids (pKLV-U6gRNA(sgRNA)-PGKpuro2ABFP). Two days after infection, Pfa1\_Cas9 cells were sorted on a BD Bioscience FACSARIA II using Blue Fluorescent Protein (BFP) as a marker.

Instrument

FACS Canto II, BD Biosciences and BD Bioscience FACSARIA II

Software

For data collection the BD FACS DIVA software was used.  
For data analysis FlowJo (Version 10) software was used.

Cell population abundance

The abundance of the desired cell population in post-sort fractions was generally > 96 % of the total post sort population. Sorting was performed using the 4-way purity setting on the BD FACSARIA II.

Gating strategy

Live cell populations were separated from cellular debris and dead cells using FSC/SSC.

Tick this box to confirm that a figure exemplifying the gating strategy is provided in the Supplementary Information.